Neurogenetic evidence for oscillatory behavior of Lgr3-positive growth control interneurons in *Drosophila*

Rebeca Zanini[1,2*], Joana Pereirinha[2,3*], Magdalena Fernandez-Acosta[2,4], Andreia P. Casimiro[2], Mariana Pinho[2], Andres Garelli[1,2,5], Fabiana Herédia[1,2#], Alisson M. Gontijo[1,2#]

[1] cE3c - Centre for Ecology, Evolution and Environmental Changes & CHANGE - Global Change and Sustainability Institute, Department of Animal Biology, Faculty of Sciences, University of Lisbon, Lisbon, Portugal.
[2] iNOVA4Health, Nova Medical School, Faculdade de Ciências Médicas, NMS, FCM, Nova University of Lisbon, Lisbon, Portugal.
[3] Institute of Molecular Biology, Mainz, Germany.
[4] Laboratorio de Genética del Comportamiento, Fundación Instituto Leloir - Instituto de Investigaciones Bioquímicas de Buenos Aires (IIBBA- CONICET), Buenos Aires, Argentina.
[5] Instituto de Investigaciones Bioquímicas de Bahía Blanca (INIBIBB), CONICET and Departamento de Biología, Bioquímica y Farmacia, Universidad Nacional del Sur, Bahía Blanca, Argentina.

* These authors contributed equally to this work.

Corresponding authors: fdheredia@ciencias.ulisboa.pt; amgontijo@ciencias.ulisboa.pt

ABSTRACT

The ability of animals to achieve a species-specific size and proportion even in the face of developmental or environmental perturbations is termed developmental stability. In *Drosophila*, the relaxin/insulin-like peptide 8 (Dilp8) mediates interorgan growth coordination during larval development acting upstream of the neuronal relaxin-like Leucine-rich repeat-containing G protein-coupled receptor (Lgr3). Previous reports have led to a model where Dilp8-dependent Lgr3 activation in two bilateral brain interneurons termed *pars intercerebralis* Lgr3-positive/growth-coordinating Lgr3 (PIL/GCL) neurons leads to their depolarization, which then triggers a neuroendocrine cascade that promotes developmental stability by delaying the larval-to-pupal transition and reducing organ growth concomitantly. However, many fundamental aspects of this model remained to be experimentally proven, most notably the specific requirement of Lgr3 and depolarization in PIL/GCL neurons for developmental stability. Here, we confirm the first part of the model regarding the specific requirement of Lgr3 in PIL/GCL neurons using improved genetic drivers, but, in contrast to the model predictions, we find that both hyper- and depolarized states of these neurons are required for their developmental delay-promoting activity in response to Dilp8. The simplest explanation for this finding is that Lgr3 activation by Dilp8 triggers oscillatory activity of PIL/GCL neurons, and that this is required for the Dilp8-dependent developmental delay. Whether or not such oscillatory behavior would arise from intrinsically pacemaker activity or from network connectivity properties such as feedback inhibition remains to be defined, although we present evidence that both could be involved. Namely, PIL/GCL neurons are positive for Cyclin A, which has been linked with sleep time coordination in adult postmitotic neurons. On the other hand, the neuroanatomy of PIL/GCL neurons is consistent with reciprocally-innervating loop-forming neurons, a common architecture in oscillating circuits and central pattern generators. Finally, we demonstrate through clonal analyses that PIL/GCL neurons represent two distinct neuronal types–a local and a projection neuron–instead of a homogeneous neuronal population as previously thought, revealing a new complexity layer in the developmental stability circuit. Our findings highlight the importance of cell-type specific neurogenetic manipulation, detailed neuroanatomical characterization, and reveal a critical and unanticipatedly complex role for PIL/GCL neurons in the Dilp8-dependent developmental stability pathway.

INTRODUCTION

Animals coordinate the growth of their body and body parts using both local and systemic programs to reach a species-typical final size and proportion [1-5]. The robustness of this process against intrinsic or environmental perturbations is termed developmental stability [1- 2, 6-7]. In *Drosophila*, the relaxin/insulin-like peptide 8 (Dilp8) mediates interorgan growth coordination during larval development [8-10]. Dilp8 is produced and secreted from larval peripheral epithelial tissues called imaginal discs (larval precursors of adult appendages such as eyes, legs, and wings) undergoing growth stresses, such as during tumorigenesis or regeneration. Dilp8 activity promotes developmental stability by delaying the onset of metamorphosis, which terminates disc growth. This delay provides extra time for the discs to compensate for their abnormal growth [11] and in its absence, animals accumulate developmental errors and/or die [8,10, 12-15] Dilp8 activity depends on the presence of the relaxin receptor-like protein, Leucine-rich repeat-containing G protein-coupled receptor (Lgr3), in larval neurons [16-19]. Two bilateral brain interneurons, named *pars intercerebralis Lgr3*-positive (PIL)/growth coordinating *Lgr3* (GCL) neurons, hereafter referred to as PIL/GCL neurons, have been hypothesized—but not functionally tested—to be the critical neurons mediating the Lgr3-dependent response to the Dilp8 peripheral tissue stress signal [10,16-18] (**Figure 1A**). This hypothesis is based

on the following main pieces of evidence: 1) the Dilp8-dependent delay in the onset of pupariation can be suppressed by RNAi-mediated knock-down of *Lgr3* using GAL4-dependent gene drivers that drive expression in subpopulations (hundreds) of neurons that include the PIL/GCL neurons. Namely, these are the *GMR19B09-GAL4* driver, hereafter referred to as *R19B09>* [a ~3.7-kb *cis*-regulatory motif (CRM) corresponding to the 7th intron and part of the flanking exons of the *Lgr3* locus [16-18,20]; **Figure 1B**], *Lgr3-GAL4::VP16* [where *GAL4::VP16* was inserted into a BAC containing the whole *Lgr3* gene plus ~1-kb upstream and 6.6-kb downstream sequence, substituting the first exon of *Lgr3* and carrying its own new 3'UTR [16], and *MZ699-GAL4* [*MZ699>*, an unmapped *GAL4* enhancer trap [17-21]. *MZ699* and *R19B09* overlap in at least 9 bilateral cells in the central nervous system (CNS) [17], whereas an intersection between *R19B09>* and *Lgr3-GAL4* is reported to overlap only in PIL/GCL neurons [16] which might be a matter of assay sensitivity as *Lgr3-GAL4* supposedly recapitulates expression from the whole *Lgr3* locus, which should include some or all of the *R19B09>* pattern that by itself drives detectable expression in a couple of hundreds of neurons [17]. Importantly, neither intersection was yet used to manipulate *Lgr3* activity and therefore test the hypothesis that *Lgr3* is required in the intersecting cells, and if so, in which of these cells. 2) Silencing of *Lgr3* in a substantial amount of ventral nerve cord (VNC) neurons using the *teashirt* (*tsh*)-*GAL4* driver, which drives expression in most VNC neurons with the notable exception of those in the segments A8/9, does not rescue the Dilp8-developmental delay caused by constitutive expression of *dilp8* under the control of a *tubulin* promoter (*Tub-dilp8*), suggesting that the critical cells that require Lgr3 to convey the Dilp8 response are located in the brain (such as the PIL/GCL neurons) or in segments A8/9 [18]. 3) Ubiquitous expression of Dilp8 activates gene expression from a cAMP (and Ca^{2+})-responsive element (CRE) reporter in PIL/GCL neurons[17-18], and this activation is dependent on neuronal *Lgr3* [18], as panneuronal RNAi against *Lgr3* abrogates reporter activity in PIL/GCL neurons. Critically, whether or not this response is important or not for the Dilp8 response was never investigated. 4) Neuronal silencing of *R19B09>*- or *MZ699>*-positive cells by driving the human *inwardly-rectifying potassium channel KCNJ2* [*Kir2.1* [22,23] partially suppresses the tissue-damage-induced delay in the onset of metamorphosis [17], whereas the expression of the *Bacillus halodurans sodium channel NaChBac* under the control of *R19B09>* (which should cause electrical hyperexcitation of neurons) caused a delay in the onset of metamorphosis [18].

Hence, the accepted model is that Lgr3 receptor activation in the PIL/GCL neurons leads both to an increase in cAMP signaling and to PIL/GCL neuron activation by membrane depolarization and supposedly release of neurotransmitters to downstream neurons (**Figure 1C**). Activated PIL/GCL neurons then send inhibitory signals, probably via other neurons, such as PTTH neurons [16-18], which antagonize the biosynthesis of ecdysone by the ring gland, causing a delay in the onset of metamorphosis (**Figure 1A**).

As mentioned above, despite these findings and model, there are no reports describing the manipulation of *Lgr3* activity exclusively in PIL/GCL neurons to determine if these are indeed neurons responsible for the developmental-delay activity of the Dilp8-Lgr3 pathway. An alternative model is that Lgr3 is required in other neurons or in other neurons in addition to the PIL/GCL neurons. Similarly, cAMP activity has not yet been functionally implicated in the Dilp8 delay in these neurons, as an alternative interpretation of the results above would be that the Dilp8- and Lgr3-dependent CRE activation observed previously could be an artifact of the tools used and/or a true biological response to Dilp8-Lgr3 pathway activation, which is nevertheless unnecessary for the Dilp8-Lgr3 pathway function on developmental stability *per se*. Finally, the activity of the PIL/GCL neurons has not been separately and exclusively genetically manipulated to test the model. Therefore, the question of what occurs downstream of Lgr3 activation at the neuronal-activity level remains open. Without direct tools to

exclusively manipulate these neurons, the current model (**Figure 1C**) could be partially or completely incorrect, as the previously reported neuronal activity manipulations involved populations of hundreds of neurons.

Here, we used functional enhancer bashing and intersectional genetic experiments coupled with RNA interference (RNAi) and neurogenetic manipulations to test several aspects of this model. We generate PIL/GCL neuron genetic drivers with increased specificity and provide definitive functional evidence that removal of Lgr3 in PIL/GCL neurons is sufficient to abrogate the developmental-delay activity of Dilp8, confirming the first part of the model. We also provide the first genetic evidence that a cAMP increase in neurons via stimulatory G protein (G_s) signaling is required for this Dilp8 activity, which is also consistent with the current model. However, in contrast to the current model, where Dilp8-triggered PIL/GCL-neuron depolarization was thought to delay the larval-to-pupal transition, we find that both hyper- and depolarized states are required for the developmental delay-promoting activity of these neurons in response to Dilp8. The simplest interpretation of these findings posits a model where Dilp8 triggers oscillatory behavior of PIL/GCL neurons in an Lgr3- and G_s-dependent-manner, and that PIL/GCL membrane potential oscillation is critical to delay the larval-to-pupal transition and promote developmental stability. Immunohistochemistry and neuroanatomical studies provide an initial indication that the oscillation mechanism might involve Cyclin A (CycA), which has been previously linked to sleep length coordination in postmitotic neurons of adult flies [24-25], and/or reciprocal loop network properties, widely known to mediate rhythmically-active neuronal networks (reviewed in [26-27]), respectively. Our results, apart from highlighting the importance of cell-type specific neurogenetic manipulations, reveal an unexpectedly complex role for PIL/GCL neurons in the Dilp8-dependent developmental stability pathway, provide new mechanistic insight to it, and point to an involvement of the Dilp8-Lgr3 relaxin-like pathway in the control of rhythmically active neuronal networks.

RESULTS AND DISCUSSION

DISSECTION OF THE R19B09 ENHANCER

R19B09 enhancer bashing identifies at least two independent cis-regulatory motifs capable of driving gene expression in cells requiring Lgr3 for the Dilp8-dependent delay

To start testing the model where Lgr3 is required in PIL/GCL neurons for the developmental delay in response to the Dilp8 peripheral stress signal, we attempted to generate PIL/GCL neuron-specific drivers to specifically manipulate these neurons using independent strategies. The first strategy consisted of enhancer bashing. As described above, the *Lgr3 R19B09* CRM/enhancer drives expression in a subpopulation of neurons that definitely contains the critical cells requiring *Lgr3* function to convey the Dilp8-dependent delay [16-19], and also cells that produce a developmental delay when depolarized [18]. Of the ~270 *R19B09*>-expressing neurons [17,28], four are the PIL/GCL neurons [16-18]. *R19B09* was previously bashed into smaller partially-overlapping segments (*R19B09.1, R19B09.2*, and *R19B09.3*–the latter being further bashed into 5 fragments *.3A-E*) each of which was placed upstream of GAL4 (**Figure 1D**), and their expression pattern was characterized in the adult CNS [29], but not in the larval CNS. Here, we used these constructs to try to pinpoint the *R19B09* segment(s) that drive(s) expression in larval neurons where Lgr3 is necessary to convey the Dilp8-dependent delay and/or segment(s) that drive(s) expression in PIL/GCL neurons. Our hypothesis was that these will be the same, as is expected in the model (**Figures 1A and C**). The alternative is that the PIL/GCL neurons

might not be the critical cells in which Lgr3 is required for the Dilp8-dependent delay, so that the fragments we identify while answering both questions might differ.

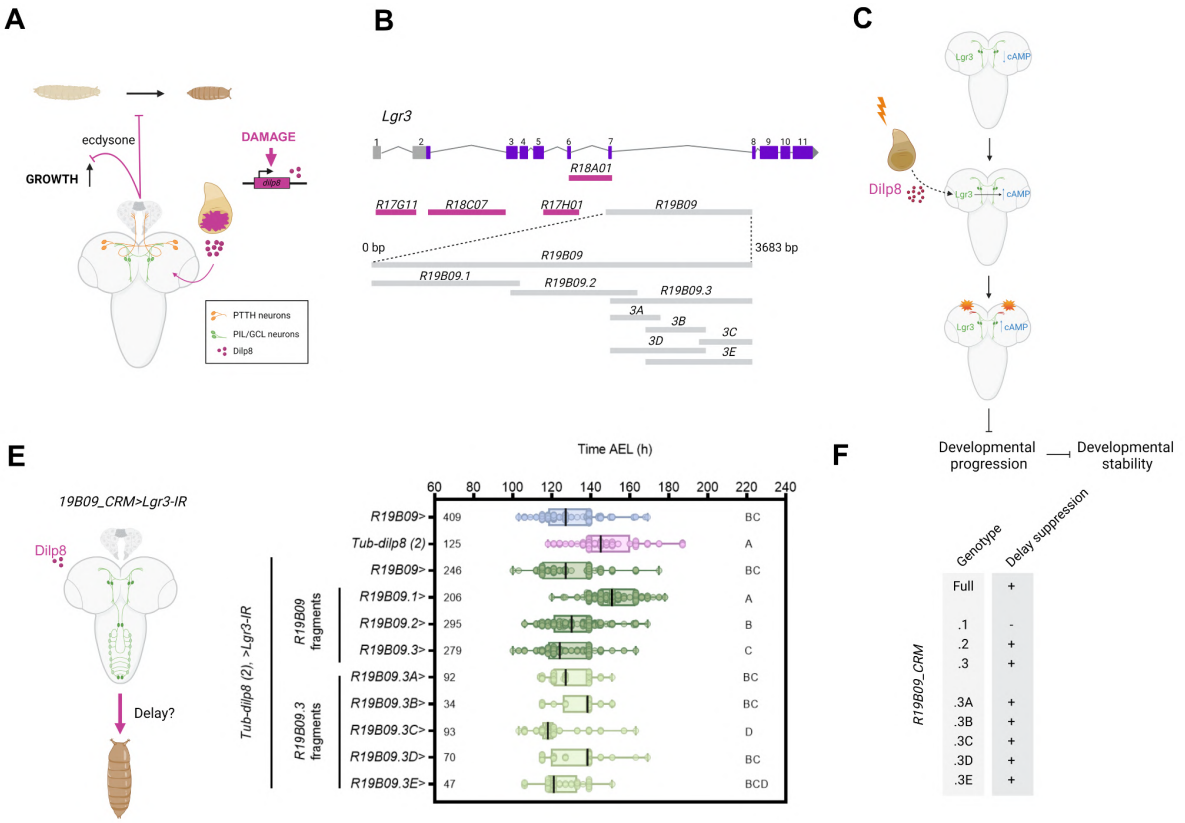

Figure 1. Enhancer bashing identifies specific fragments driving expression in cells requiring Lgr3 for the Dilp8-dependent developmental delay. (A) Model of the Dilp8-Lgr3 pathway for developmental stability in *Drosophila*. Scheme adapted from [10]. Dilp8 secreted from abnormally-growing imaginal discs indirectly inhibits ecdysone production, whose lower levels promotes developmental stability by delaying the transition from larval to pupal stage, allowing more time for imaginal discs to fine-tune their growth. **(B)** Schematic representation of the *Lgr3* gene. Five large non-coding regions (introns) of the *Lgr3* gene (*R17G11*, *R18C07*, *R17H01*, *R18A01*, and *R19B09*), containing putative *Lgr3 cis*-regulatory motifs (CRMs) have been placed upstream of *GAL4*, and their expression in the CNS has been characterized at FlyLight [20,29]. *R19B09* (green bar), but not the other drivers (magenta bars), drives expression in a population of cells, englobing the PIL/GCL neurons, in which Lgr3 is necessary to transduce the Dilp8-dependent delay [16-19]). **(C)** The current model of Lgr3-dependent activity in PIL/GCL neurons suggests that these are in an inactive state (inactive zone, blue) with low concentrations of intracellular cAMP, until Lgr3 is activated by the Dilp8 peripheral tissue stress signal. This activation leads to an increase of cAMP followed by membrane depolarization and synaptic activation (orange star represents synaptic activation; active zone, orange). In this model, PIL/GCL neuron activation induces a delay in developmental progression (larval to pupal transition), which promotes developmental stability. **(D)** *R19B09* was divided into multiple fragments, each of which was also placed upstream of *GAL4* [30]. Here, we used these fragments to map the *R19B09* region(s) that drive(s) expression in cells where Lgr3 is necessary to convey the Dilp8-dependent delay and/or region(s) that drive(s) expression in PIL neurons. *R19B09* was bashed into three approximately equal fragments (*R19B09.1-3*), with fragment *R19B09.3* being further dissected into three parts (*R19B09.3A-C,* with *R19B09.3D* and *.3E* encompassing 3A+B and 3B+C, respectively). **(E)** Functional dissection of the *R19B09* CRMs identifies two independent regions that redundantly control *Lgr3* expression in cells that are relevant for the Dilp8-dependent delay. Box plot showing pupariation time (Time after egg laying (AEL)) in h of (N) larvae expressing *dilp8* under the control of *Tubulin* promoter (*Tub-dilp8(2),* a 2nd-chromosome insertion) and RNAi against *Lgr3* (*Lgr3-IR*) under control of the *Lgr3* CRM, *R19B09* (*R19B09>*, control for suppression), and various *R19B09* fragments. As a negative control, a stock carrying *R19B09>* was crossed with *w[1118]* animals, and F1 larvae were scored (blue). As a positive control for the delay, *Tub-dilp8, UAS-Lgr3-IR* animals were crossed with *w[1118]* animals, and F1 larvae were scored (magenta). Whiskers extend to minimum or maximum values. Each dot represents one individual. The vertical bars represent the median. $P < 0.0001$, One-way ANOVA test. Genotypes sharing the same letter are not statistically different at $\alpha = 0.05$, Tukey's *post-hoc* test. **(F)** Summary of the phenotype of *Tub-dilp8* suppression for each *R19B09* fragment. In the table, "+" denotes a positive finding, and "-" denotes a negative finding.

To answer the first question of which *R19B09* region(s) drive(s) expression in cells where Lgr3 is necessary to convey the Dilp8-dependent delay, we expressed RNAi against *Lgr3* (*Lgr3-IR* [30]) under the control of the different *R19B09 CRM-GAL4* (*R19B09_CRM>*), and assayed for their ability to suppress the delay produced by constitutive expression of *dilp8* using *Tub-dilp8(2)* (an insertion on the 2nd chromosome [18]) (**Figure 1E**). Consistent with previous results [17], *Tub-dilp8(2)* induced an 18-h median delay relative to controls ($P < 0.0001$, Tukey's *post-hoc* test), and the *R19B09>* control driver significantly rescued this delay when driving *Lgr3-IR* ($P < 0.0001$, for both, Tukey's *post-hoc* test). These results further corroborated previous results showing that the Lgr3 receptor is necessary in *R19B09>*-expressing cells to delay the onset of metamorphosis in response to Dilp8 [16-19]. Regarding the *R19B09* fragments, all fragments, except *R19B09.1*, showed significant suppression of the Dilp8-induced delay when driving *Lgr3-IR* ($P < 0.0001$, Tukey's *post-hoc* test). As the *R19B09.3A* and *R19B09.3C* regions correspond to non-overlapping segments of the seventh intron of *Lgr3* (**Figure 1B and D**), our result suggested there are at least two independent fragments within the *R19B09* element driving gene expression in cells requiring Lgr3 for the Dilp8-dependent delay. *Drosophila Lgr3* has hence evolved at least two enhancers in its seventh intron to secure Lgr3 protein expression in the cells required for the Dilp8-dependent delay. Whether or not these fragments drive redundant gene expression in the same population of Lgr3-positive, Dilp8-sensitive cells or not, and whether or not these are PIL/GCL neurons, cannot be concluded from these experiments alone.

The R19B09 CRMs that independently drive expression in the cells required for the Dilp8-dependent delay are shadow enhancers for the PIL/GCL neurons

To answer the second question of which *R19B09* segment(s) drive(s) expression in PIL/GCL neurons, we expressed membrane-targeted *myristoylated* (*myr)::tdTomato* [31] under the control of the different *R19B09* fragments in animals carrying the endogenous *Lgr3* translational reporter, *super folder green fluorescent protein*::*Lgr3* (*sfGFP::Lgr3*), which labels all Lgr3-positive neurons, including the PIL neurons [17] (**Figure 2A-B**). We crossed the different *R19B09_CRM>* lines with a stock carrying *UAS-myr::tdTomato; sfGFP::Lgr3*, and then performed immunohistochemistry of the F1 larval CNS to analyze the colocalization between *sfGFP::Lgr3* and *myr::tdTomato*, detected with an antibody against green fluorescence protein (GFP) and the endogenous tdTomato fluorescence, respectively. Therefore, when the *R19B09_CRM>* drives expression in the PIL neurons, we expect to observe a colocalization of both reporters. Our results show clear colocalization between *sfGFP::Lgr3* and *myr::tdTomato* driven either by *R19B09.3>* or by its five subfragments (*R19B09.3A-E*) (**Figure 2A**). Interestingly, these results show that PIL/GCL neuron expression is regulated by two independent and redundant CRMs contained in the non-overlapping fragments *R19B9.3A* and *R19B09.3C*. Redundant CRMs can be called shadow enhancers [32]. *Drosophila Lgr3* has hence evolved at least two shadow enhancers in its seventh intron to secure Lgr3 protein expression in the PIL/GCL neurons. Shadow enhancers can confer precision and robustness to gene expression, albeit complete spatial redundancy is rare [33]. Consistent with this, *R19B9.3A>* and *R19B09.3C>* seem to drive different patterns aside from the coinciding PIL neuron expression (**Figure 2A**).

Contrary to *R19B09.3>*, neither *R19B09.1>* nor *R19B09.2>* drove detectable expression of *myr::tdTomato* in the PIL/GCL neurons. As the *R19B09.1>* driver also does not suppress the Dilp8-dependent delay when driving *Lgr3-IR*, we can also conclude that Lgr3 is not required in *R19B09.1>*-expressing cells, to convey the delay. However, in contrast to *R19B09.1>*, the *R19B09.2>* driver suppresses the Dilp8-dependent delay when driving *Lgr3-IR*. These initial results opened up the possibility that, contrary to the current model and our expectations, the PIL/GCL neurons may not be

the cells or may not be the only cells requiring Lgr3 in the Dilp8 pathway to induce a developmental timing delay.

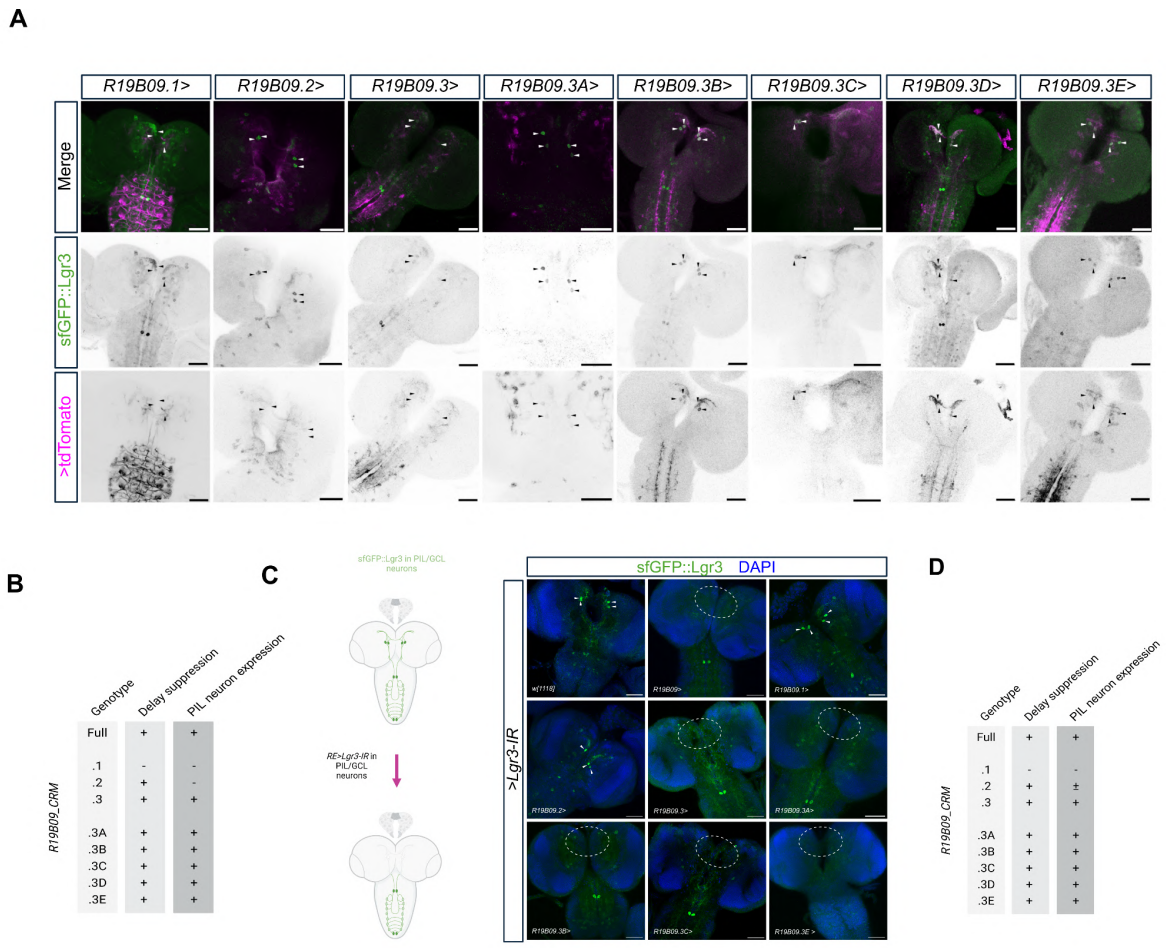

Figure 2. ***Lgr3 R19B09.3 CRM*s drive expression in PIL neurons. (A)** Sum of confocal z-stack slices stained with anti-GFP (green) to show *sfGFP::Lgr3* expression. Endogenous *myr::tdTomato* fluorescence driven by the various *R19B09_CRMs* is labeled in magenta. DAPI counterstain labels nuclei (blue). Both *R19B09.1>* and *R19B09.2>* do not drive detectable expression in sfGFP::Lgr3-positive PIL/GCL neurons, while the *R19B09.3>* fragments do. PIL/GCL neuron cell bodies are highlighted with arrowheads. **(B)** Summary of the phenotypes of *Tub-dilp8* suppression and PIL neuron expression for each R19B09 fragment. In the table, "+" denotes a positive finding and "-'' denotes a negative finding. **(C)** Two independent CRMs within the R19B09 element drive gene expression in the PIL/GCL neurons. Sum of confocal z-stack slices stained with anti-GFP (green) and DAPI (blue). The CRMs drive *Lgr3-IR,* reducing the *sfGFP::Lgr3* expression (green) in the subset of cells where they are expressed. As a negative control, we crossed *w[1118]* animals to *UAS-Lgr3-IR-V22, sfGFP::Lgr3* animals, so that *Lgr3-IR* is not expressed in this condition, and all sfGFP::Lgr3-positive neurons are labelled in green. As a positive control, we used *R19B09>* driving *Lgr3-IR*, expecting the absence of *sfGFP::Lgr3* in the PIL/GCL neurons. In the images where no PIL/GCL-like neurons are detectable, a white dashed circle denotes the anatomical region where their soma would otherwise be typically located. **(D)** Summary of the phenotypes of delay suppression and PIL neuron expression (summary of PIL neuron expression findings using both *sfGFP::Lgr3 Lgr3-IR* and *sfGFP::Lgr3 myr::tdTomato* colocalization techniques) for each R19B09 fragment. In the table "+" denotes a positive finding and "-'' denotes a negative finding. Scale bars, 50 µm.

Intrigued by the findings described above, we reasoned that our results could also be explained by the different sensitivity of the assays used above. Namely, that in the *Tub-dilp8*-delay experiments, certain *R19B09_CRM* drivers, such as the *R19B09.2>*, could drive very low levels of *Lgr3-IR* in the PIL/GCL neurons, which could nevertheless be sufficient to reduce Lgr3 protein levels enough to suppress the

Dilp8-dependent delay, yet the same drivers could be too weak to lead to detectable myr::tdTomato fluorescence in the colocalization strategy. Hence, in order to independently confirm that the *R19B09.1>* and *R19B09.2>* elements do not drive expression in the PIL/GCL neurons, and that the *R19B09.3>* element does, we devised a more sensitive immunofluorescence assay to test the capability of *R19B09_CRM>*-driven *Lgr3-IR* to reduce *sfGFP::Lgr3* protein levels in the PIL/GCL neurons. Namely, we crossed animals of the genotype *UAS-Lgr3-IR-V22, sfGFP::Lgr3* with the different *R19B09_CRM>* lines, and performed immunofluorescence analyses on dissected CNSs from the F1 larvae of the genotype *R19B09_CRM>Lgr3-IR; sfGFP::Lgr3*, using an antibody against GFP. Consistent with the results above using the myr::tdTomato reporter, virtually no detectable *sfGFP::Lgr3* was observed in cell bodies located in the PIL/GCL neuron anatomical region when *R19B09.3>* was used to express *Lgr3-IR* [0.08 ± 0.28, Mean ± standard deviation (SD) PIL/GCL neurons/brain; only 1 out of 13 brains had 1 PIL/GCL neuron detectable] (**Figure 2C-D**). Qualitatively similar results were found for all *R19B09.3>* subfragments tested, including *R19B09.3A>* and *R19B09.3C>* (**Figure 2C-D**). These results confirm that *R19B09.3>* and both *R19B09.3A>* and *R19B09.3C>* shadow enhancers drive expression in the PIL/GCL neurons, and that this expression is sufficiently strong to reduce endogenous Lgr3 protein levels to undetectable levels when driving *Lgr3-IR*.

In contrast, when *Lgr3-IR* was driven under the control of *R19B09.1>,* we could still observe PIL/GCL neurons expressing *sfGFP::Lgr3* in all surveyed preparations (3.90 ± 0.30 PIL/GCL neurons/brain, *N* = 11 brains), suggesting that this segment does not drive significant GAL4 expression in PIL/GCL neurons. This result is consistent with our previous observation on the lack of colocalization between *sfGFP::Lgr3* and *R19B09-1>*myr::tdTomato (**Figure 2A**). Interestingly, and in contrast, when we looked at *R19B09.2>Lgr3-IR* brains, *sfGFP::Lgr3* expression in PIL/GCL neurons apart from seeming weaker compared to brains of *R19B09.1>Lgr3-IR* animals*,* only a fraction of the four PIL/GCL neurons were present (2.16 ± 1.16 PIL/GCL neurons/brain, *N* = 6), suggesting that *R19B09.2>* drives weak, yet biologically-effective (capable of reducing endogenous Lgr3 protein levels) gene expression in PIL/GCL neurons. This very likely explains why *R19B09.2>*-driven *Lgr3-IR* is sufficient to suppresses the Dilp8-dependent delay **(Figure 1C-D)**, and also provides an initial indication that the collective activity of the PIL/GCL neurons is critical for a proper response of Lgr3-positive neurons to the Dilp8 developmental-delay promoting signal. The fact that we could not see colocalization between R19B09.2>myr::tdTomato and sfGFP::Lgr3 **(Figure 2A-B)**, could be explained by a weaker sensitivity of the colocalization assay–*i.e.,* such that the expression of *myr::tdTomato* is too weak to be detected in our staining conditions. Our results up to now are highly consistent with the model that PIL/GCL neurons are the cells where Lgr3 is required to transduce the Dilp8-dependent delay.

R19B09 enhancer bashing identifies an incongruence between cells requiring Lgr3 and those inducing a developmental delay when depolarized

Previous work has shown that depolarization of *R19B09*-positive neurons using the NaChBac sodium channel was sufficient to delay the onset of metamorphosis [18]. If the PIL/GCL neurons are indeed the neurons causing such a delay, as hypothesized in the current model (**Figure 1A and C**), then the neurogenetic activation of all *R19B09_CRM>*-positive cells except *R19B09.1* should cause a delay in development. To address this, we first attempted to independently replicate the finding above by thermogenetically activating *R19B09*-positive neurons expressing the transient receptor potential cation channel A1 ortholog (TrpA1) with a temperature shift from 18°C to 29°C at the second larval instar stage **(Figure 3A)**. To further test the epistatic relationship between neuronal activation and Lgr3 requirement, we performed these experiments in the presence or not of *Lgr3* RNAi. For this, we scored the timing of pupariation of F1 larvae of *R19B09>* animals crossed with three different stocks: *UAS-*

Lgr3-IR, a condition where we do not expect a delay in the onset of metamorphosis; *UAS-TrpA1,* where *TrpA1* is driven, leading to cation influx in the cells and depolarization at 29°C [34-38]; and *UAS-TrpA1; UAS-Lgr3-IR,* a condition where both *TrpA1* and *Lgr3-IR* are driven to test their epistasis. The controls used were *R19B09>* crossed with *UAS-Lgr3-IR*, and each of the *UAS* lines crossed with *w[1118]*. The results show that *R19B09>* significantly delays the onset of metamorphosis when driving TrpA1 ($P < 0.05$, Tukey's *post-hoc* test), corroborating the previous report using an independent method of neuronal activation [18]. Furthermore, we find that the TrpA1-induced delay does not require Lgr3 in the *R19B09>*-expressing cells, because the delay is not rescued by co-expression of *Lgr3-IR* ($P > 0.05$, Tukey's *post-hoc* test). This suggests that activation of R19B09 neurons is epistatic to Lgr3 activity in these neurons. One possibility is that R19B09-positive neuronal firing occurs downstream of Lgr3 activation by Dilp8, hence neuronal Lgr3 becomes dispensable. This is consistent with the current proposed model.

Next, we attempted to confirm if the PIL/GCL neurons are responsible for the R19B09>TrpA1-induced delay. Our strategy was to thermogenetically activate the different subsets of *R19B09>*-expressing cells using the different *R19B09_CRM>* lines crossed to *UAS-TrpA1* and score the timing of pupariation in similar temperature-shift conditions as the experiments described above **(Figure 3B-C)**. As a positive control for the TrpA1-induced delay, we used the complete *R19B09* element driving *TrpA1* (*R19B09>TrpA1*). The results showed that all *R19B09_CRM>* drivers, except *R19B09.3A>*, induced some extent of statistical significant delay in pupariation time when compared with the *UAS-TrpA1* negative control *R19B09* driver ($P < 0.05$, Tukey's *post-hoc* test) (**Figure 3B-C**). The weakest lines were *R19B09.1>* and *R19B09.2>* (~9-h median delays relative to control, $P < 0.05$, Tukey's *post-hoc* test for both). As all *R19B09.3* subfragments, except for the *R10B09.3A*, induced stronger delays upon TrpA1 activation (19.3 ± 4.3 h, average median delay ± SD), we interpret these results as indicative that the most relevant TrpA1-sensitive cells are part of the population of cells in which elements located at the two distal thirds of the *R19B09* element (represented by the CRM segments *R19B09.3, 3B, 3C, 3D,* and *3E*) are active. The fact that *R19B09.3A>*-expressing cells do not induce a delay when thermogenetically activated despite being clearly active in PIL/GCL neurons (**Figure 1B and Figure 2A-B**), proposes two mutually exclusive scenarios. One is that thermogenetic activation of PIL/GCL neurons is sufficient to induce a delay, but it is blocked by depolarization of other neurons uniquely present in *R19B09.3A>*. In the alternative scenario, the thermogenetic activation of PIL/GCL neurons is not sufficient to induce a delay, and the experimentally extended larval period is the consequence of thermogenetic activation of other, yet unidentified cells, labeled by some *R19B09* elements (e.g. *R19B09.3B*) and absent in *R19B09.3A*. If this is the case, it would be very interesting to determine in future work if these cells are part of the Dilp8- and Lgr3-dependent developmental stability pathway or rather represent cells acting in other pathways relevant for developmental timing control [3-4].

In summary, enhancer bashing of the *Lgr3 R19B09* CRM **(Figure 3D)** led to the four main conclusions: 1) that at least two PIL/GCL-neuron shadow enhancers are present in the *Lgr3* gene; 2) there is a correlation between the *R19B09* CRM subfragments that drive expression in cells requiring *Lgr3* for the Dilp8-dependent delay and those that drive expression in PIL/GCL neurons; 3) that a small *R19B09* region (*R19B09.3A*) that drives expression in PIL/GCL neurons is not sufficient to induce a delay upon thermogenetic activation; and 4) that other R19B09-positive cells, not marked by the driver *R19B09.3A>*, which excludes the PIL/GCL neurons, can delay the larval-to-pupal transition upon thermogenetic activation and in an *Lgr3*-independent manner.

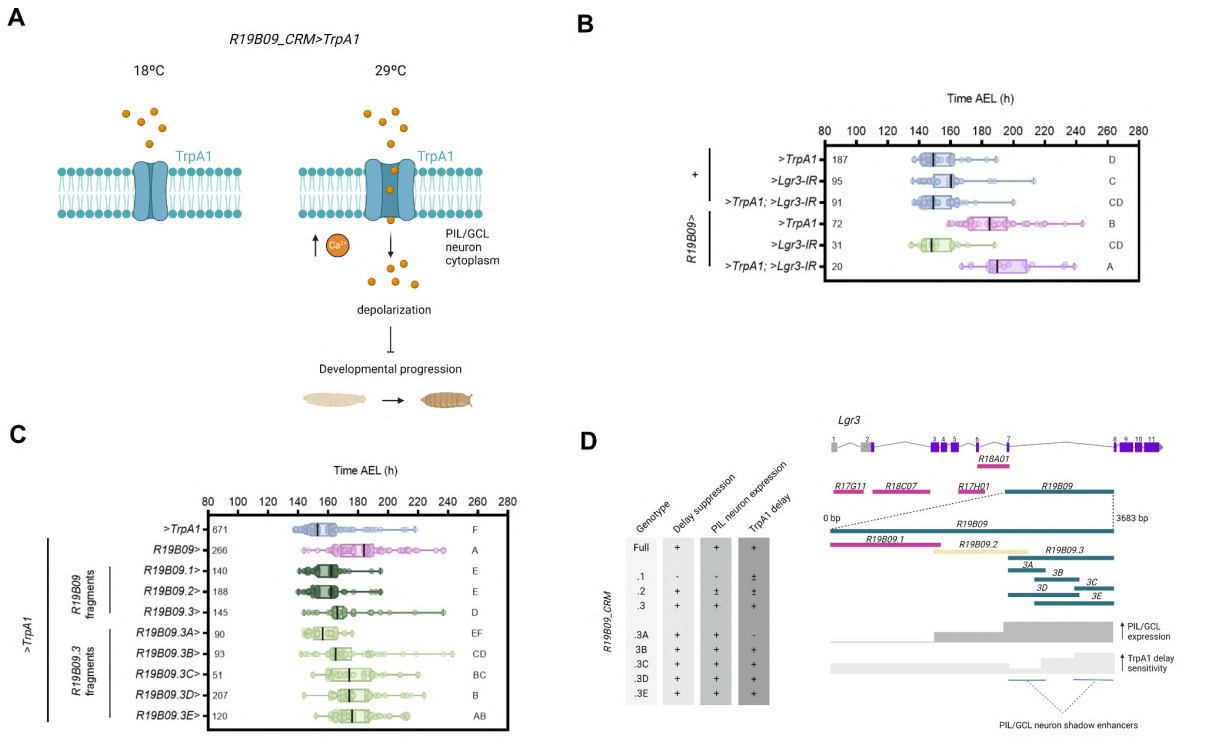

Figure 3. *Lgr3 R19B09.3* CRMs drive expression in TrpA1-sensitive cells, inducing a developmental timing delay. (A) Scheme depicting the experimental design for testing the sensitivity of the different cell populations marked by the *R19B09_CRMs* to the temperature-dependent Trpa1 neuronal activation. The final readout is timing of the larva to puparium transition (Developmental progression). Temperature-dependent TrpA1 activation (29 C) in PIL/GCL neurons will lead to cation influx (such as Calcium ions (orange circles) and neuronal despolarization, which is predicted to lead to a delay in the larval to pupariation transition according to the current model (**Figures 1A and C**). **(B)** Box plot showing pupariation time (Time after egg laying (AEL)) in h of (N) larvae expressing the transient receptor potential cation channel A1 ortholog (*TrpA1*) and *Lgr3-IR* under the control of the *Lgr3 R19B09* (*R19B09*>) driver. As negative control for delay, the same UAS lines were crossed with *w[1118]*. **(C)** Box plot showing pupariation time of larvae expressing *TrpA1* under the control of the various *Lgr3 R19B09_CRM* drivers. As negative control for delay, *TrpA1* was crossed with *w[1118]*. **(D)** Summary of the phenotypes of delay suppression, PIL/GCL neuron expression (summary of PIL/GCL neuron expression findings using both sfGFP::Lgr3 Lgr3-IR and sfGFP::Lgr3 myr::tdTomato colocalization techniques) and TrpA1 delay for each *R19B09_CRM* fragment. In the table "+" denotes a positive finding and "-" denotes a negative finding. The *Lgr3* gene has at least two shadow enhancers that are active in the PIL/GCL neurons. The *R19B09* CRM was fragmented into three small elements: the *R19B09.1* fragment (magenta bar), which neither regulates the response to Dilp8 in Lgr3-positive neurons nor drives expression in PIL/GCL neurons; the *R19B09.2* fragment (yellow bar), which suppresses the Dilp8-dependent delay when driving *Lgr3-IR*, but its expression in PIL/GCL neurons is weak (PIL/GCL neuron expression, dark gray); and the *R19B09.3* fragment and its subfragments (dark cyan bars), which drive *Lgr3* in cells that regulate the Dilp8-dependent delay and drive expression in the PIL/GCL neurons, constituting at least two redundant "shadow" enhancers. The capability of the cells where these CRMs are active to cause a delay upon TrpA1 activation (TrpA1-sensitivity, light gray) increases more towards the 3' region of the *R19B09.3* CRM with a possible dip around the *R19B09.3A* CRM region. In all box-plot panels, whiskers extend to minimum or maximum values. Each dot represents one individual. The vertical bars represent the median. $P < 0.0001$, One-way ANOVA test. Genotypes sharing the same letter are not statistically different at $\alpha = 0.05$, Tukey's *post-hoc* test.

TARGETING PIL/GCL NEURONS BY INTERSECTIONAL GENETICS

A sparse gene driver intersection expressed in PIL/GCL neurons shows that removal of Lgr3 in PIL/GCL neurons is sufficient to abrogate its developmental delay activity

In the current model (**Figure 1A and C**), PIL/GCL neurons are strong candidates to mediate the Dilp8- and Lgr3-dependent developmental delay, but this had never been formally tested before this study. This is because PIL/GCL neurons had always been genetically manipulated together with hundreds of

other cells due to the lack of PIL/GCL neuron-specific gene drivers. The enhancer bashing experiments described above are also consistent with this model, as they showed a correlation between the *R19B09* fragments that drive expression in cells requiring *Lgr3* for the Dilp8-dependent delay and those that drive expression in PIL/GCL neurons. Nevertheless, all of the *R19B09* fragments tested still drive expression in many other cells in addition to the PIL/GCL neurons. In order to independently confirm the model, we attempted to generate sparser and more specific PIL/GCL neuron drivers using intersectional genetics. Using fluorescent reporters, we had previously shown that the gene expression driven by the elements *R19B09-LexA* (*R19B09>>*) and *MZ699>* overlaps in at least 9 bilateral cells, two of which are the PIL/GCL neurons, while the other 7 neurons are in the VNC [17]. A genetic intersection between *R19B09>>* and *MZ699>* (*R19B09* ∩ *MZ699*) would thus allow us to functionally test if the 9 neurons are indeed required for the Dilp8-dependent delay by driving *Lgr3-IR* in the intersecting cells. To achieve this, we first quantified the genetic intersection of both drivers [*R19B09* ∩ *MZ699*] using a flip-OUT technique where *R19B09>>* drives *8xLexAop2-Flipase* (*FLPL*) [31] to remove the FRT-flanked transcriptional STOP sequence from the cassette *UAS-FRT-stop-FRT-GFP::myr* [39], to drive membrane-targeted GFP. The ***R19B09 ∩ MZ699>GFP*** genetic intersection revealed an average of 16.5 ± 2.3 GFP-positive cells per hemi-CNS (average ± SD, *N* = 11 CNS preparations), not all of which were bilateral and/or consistently observed in all preparations. This number was considerably higher than the 9 bilateral neurons previously detectable by overlapping fluorescence derived from each driver activity independently [17], and could reflect the greater sensitivity of the genetic intersection method. Of these cells, 2.7 ± 0.7 (*N* = 22 hemibrains) were in the PIL/GCL neuroanatomical area (**Figure 4A**). These cells likely correspond to the two PIL/GCL neurons plus another #5 neuron (MZ699 is active in all #5 neurons, of which the two PIL/GCL neurons are a subset [17]). Furthermore, we frequently observed another brain neuron (0.9 ± 0.6 per hemisphere), positioned more posteriorly to the PIL/GCL neurons (**Supplementary Figure S1**). In the VNC, an average of 9.2 ± 0.7 VNC neurons per side were positive and sometimes a neuroblast lineage was labeled (0.4 ± 0.3 per VNC side), typically in the lateral anteriormost VNC (**Supplementary Figure S1**). To further increase the specificity towards PIL/GCL neurons and allow genetic manipulations based on the intersection, we used another flip-OUT method based on the capability of GAL80 to directly inhibit GAL4 activity [40]. In this method, a *Tub-FRT-GAL80-FRT* flip-OUT cassette was used to convert *R19B09>>FLPL* expression into GAL4-permissive clones (GAL4 being driven by the *MZ699* driver). In addition, to further restrict MZ699-GAL4 activity to the brain, where the PIL/GCL neuron cell bodies are localized, we counteracted GAL4 expression in the VNC using *tsh-GAL80*, a GAL80 enhancer trap insertion in the 5'UTR of *tsh* [41]. This intersection, "[*R19B09* ∩ *MZ699*] — *tsh>"*, is hereafter named *PIL/GCL-GAL4* (*PIL/GCL>*).

To verify if the intersection strategy worked as expected, we tested if *PIL/GCL>* indeed drove expression in PIL/GCL neurons and not in VNC neurons. For this, we crossed *PIL/GCL>* animals with a stock carrying *UAS-myr::tdTomato; sfGFP::Lgr3*, and then performed immunohistochemistry of the F1 larval CNS to analyze the colocalization between sfGFP::Lgr3 and PIL/GCL>myr::tdTomato, detected with antibodies against GFP and myr::tdTomato (anti-DsRed), respectively. We expected to observe a colocalization of both reporters in the PIL/GCL neurons and limited or no expression in other cells across the CNS, especially in the *tsh* domain of the VNC. Consistent with our expectations, our results show clear colocalization between *sfGFP::Lgr3* and PIL/GCL>myr::tdTomato in 2.36 ± 0.77 PIL/GCL neurons per brain (n=14), and limited and variable expression in other cells (**Figure 4B**). Importantly, in 11/14 brains analyzed, there was at least 1 PIL/GCL neuron labeled in both brain hemispheres. 1/14 had 2 ipsilateral PIL/GCL neurons labeled, and 2/14 had only 1 PIL/GCL neuron labeled. Based on these results alone, the PIL/GCL> intersectional driver is expected to behave similarly

or better than the *R19B09.2>* driver, which despite only driving expression in a subset of PIL/GCL neurons (**Figures 2C-D**), significantly disrupts PIL/GCL neuron function upon RNAi or thermogenetic manipulations (**Figures 1E and 3C**). To test if the incomplete intersection was a characteristic of the *PIL/GCL>* stock or rather a limitation of the sensitivity of the colocalization assay (as reported above for the enhancer bashing experiments), we used the more sensitive *Lgr3-IR, sfGFP::Lgr3* assay, and expressed *Lgr3-IR* under the control of *PIL/GCL>* (*PIL/GCL>Lgr3-IR*) in the presence of *sfGFP::Lgr3*, followed by immunofluorescence assays, as described above. We found no detectable somatic sfGFP::Lgr3 expression in the neuroanatomical region corresponding to PIL/GCL neurons (**Figure 4C**). Although this was not quantified, these results suggested that *PIL/GCL>Lgr3-IR* can be sufficiently strong to reduce Lgr3 protein levels in PIL/GCL neurons to undetectable by immunofluorescence assays in some brains, similarly to the *R19B09_CRM>* drivers. Importantly, in other neuroanatomical regions, sfGFP::Lgr3 expression was not detectably affected (**Figure 4C**), confirming the specificity of the intersection for the PIL/GCL neurons.

Next, we used *PIL/GCL>* to functionally test the hypothesis that PIL/GCL neurons are the key neurons where *Lgr3* is required to transduce the Dilp8 developmental-delay signal. For this, we expressed *Lgr3* RNAi in *PIL/GCL>* neurons (*PIL/GCL>Lgr3-IR*) and scored the timing of pupariation in the presence of ectopic Dilp8 activity via the *Tub-dip8* cassette and compared this to a series of controls (**Figure 4D**). As expected, *Tub-dilp8(2), PIL/GCL>Lgr3-IR* animals pupariated significantly before *Tub-dilp8(2)* animals or *Tub-dilp8(2), PIL/GCL>* without the *Lgr3-IR* cassette ($P < 0.05$, Tukey's *post-hoc* test). The suppression of the delay was not as extensive as the effect of *MZ699>* alone (control *PIL/GCL>* without the *FRT-GAL80* cassette), but was statistically significant ($P < 0.05$, Tukey's *post-hoc* test). This could be due to the stochastic nature of the recombinase-mediated genetic manipulation in larvae, so that not all PIL/GCL neurons would start expressing enough *Lgr3-IR* in time for a full biological effect. Nevertheless, taken together with the enhancer bashing results, these intersectional genetics experiments unequivocally demonstrate that *Lgr3* is required in the PIL/GCL neurons for the Dilp8-dependent developmental delay, thereby confirming this part of the model (**Figure 1A**).

LGR3 SIGNALING IN PIL/GCL NEURONS

Stimulatory G protein is required in R19B09 neurons for proper pupariation

Dilp8-dependent activation of Lgr3 in PIL/GCL interneurons is associated with an increase in the intracellular levels of the second messenger cyclic adenosine monophosphate (cAMP) [10,17-18]. However, the requirement of cAMP-dependent signaling for the Dilp8 and Lgr3-dependent activities has never been formally tested. G-protein-coupled receptors increase intracellular cAMP levels by activating the heterotrimeric stimulatory G protein G_s, which then activates adenylyl cyclase to increase intracellular cAMP levels and stimulate the cAMP-dependent signaling pathway [42]. To demonstrate that Dilp8-dependent Lgr3 signaling in PIL/GCL neurons requires heterotrimeric G_s, we first used RNAi to knock down the *alpha subunit of the heterotrimeric* G_s, Ga_s (Ga_s*-IR*) in PIL/CGL neurons using the *R19B09>* driver (*R19B09>*Ga_s*-IR*) in animals carrying the developmental delay-causing *Tub-dilp8(2)* transgene, and quantified the timing of pupariation of these animals and of controls. We found that *R19B09>*Ga_s*-IR* completely suppressed the *Tub-dilp8(2)*-dependent delay in the onset of metamorphosis ($P < 0.05$ Tukey's *post-hoc* test, compared to *Tub-dilp8(2)* alone; **Figure 4E**). These results are consistent with previous findings [17- 18] and strongly support a requirement for a Ga_s and

hence a cAMP-dependent transduction pathway in PIL/GCL neurons for imaginal disc growth coordination during early larval development. Unfortunately, our efforts to knock-down *Lgr3* with greater specificity in PIL/GCL neurons using the intersectional genetics strategies described above were not fruitful due to synthetic lethality of the system with the *Ga$_s$-IR* construct insertion. An alternative to overcome this limitation in future experiments could be to resort to a sparse driver from the enhancer bashing experiments, such as *R19B09.3D>*.

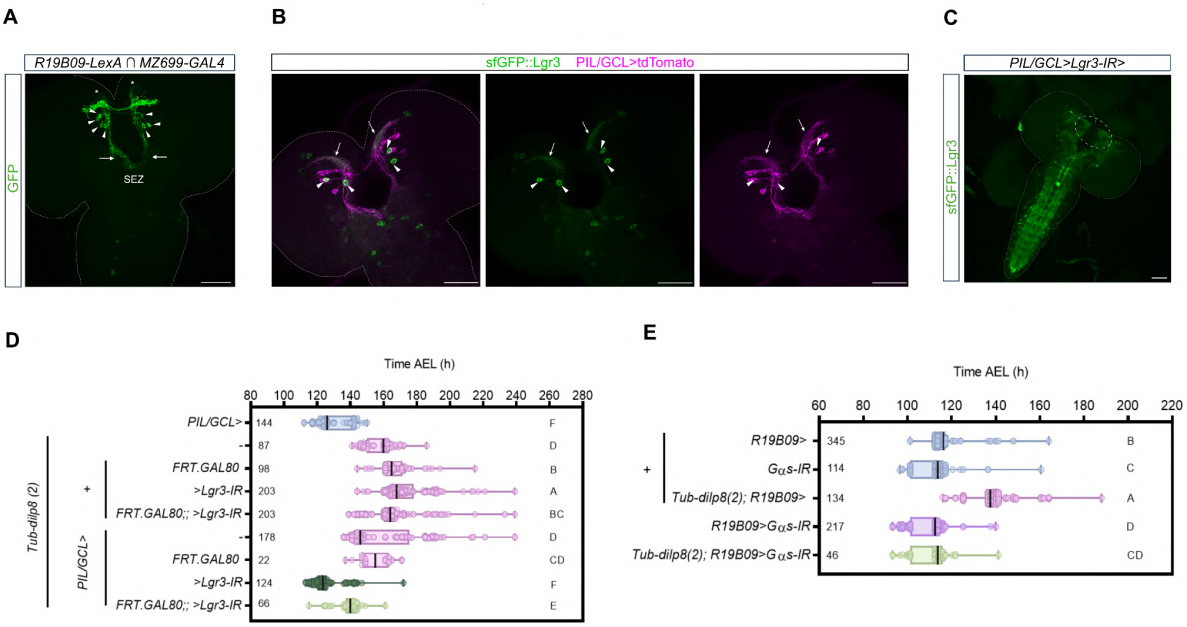

Figure 4. A sparse gene driver intersection expressed in PIL/GCL neurons shows that removal of *Lgr3* in PIL/GCL neurons is sufficient to abrogate its developmental delay activity. (**A**) The genetic intersection of *R19B09* and *MZ699* elements (*R19B09 ∩ MZ699*) reveals cells the brain region corresponding to PIL/GCL neurons. Shown is the sum of confocal z-stack slices of an immunohistochemistry preparation of dissected wandering L3 larval CNSs (anterior contour depicted with a dashed white line) expressing *R19B09 ∩ MZ699>GFP::myr* and stained with anti-GFP (green). Arrowheads point to the soma of at least seven GFP-positive neurons, with contralateral anterior arborizations (asterisks), and ipsilateral descending projections (arrows) towards the subesophageal zone (SEZ). (**B**) PIL/GCL neurons are a subset of the #5 cells labeled with *PIL/GCL>*. Depicted is the sum of confocal z-stack slices of an immunohistochemistry preparation of dissected wandering L3 larval CNSs (anterior contour depicted with a dashed white line) stained with anti-GFP (green) to show the overlap between sfGFP::Lgr3 expression and PIL/GCL>myr::tdTomato (magenta). The contralateral projections of PIL/GCL neurons occupy the anteriormost and more curvilinear region of this neuropil compartment (arborizations with green and magenta overlap, arrows). The other straighter and less arborized contralateral projections correspond to those of other neighboring sfGFP::Lgr3-negative #5 group neurons (magenta). **(C)** *Lgr3* RNAi expression under the control of *PIL/GCL>* (*PIL/GCL>Lgr3-IR*) in the presence of the *sfGFP::Lgr3* cassette leads to a complete loss of detectable anti-GFP staining in the region corresponding to PIL/GCL neurons. Shown is the sum of confocal z-stack slices of an immunohistochemistry preparation of dissected wandering L3 larval CNSs (anterior contour depicted with a dashed white line) stained with anti-GFP (green). (**D**) RNAi-mediated downregulation of *Lgr3* (*Lgr3-IR*) in PIL/GCL neurons using *PIL/GCL>* rescues the delay induced by *Tub-dilp8(2)*. Box plot showing pupariation time (Time after egg laying (AEL)) in h of (N) larvae. As a negative control, a stock carrying *PIL/GCL>* was crossed with *w[1118]* animals. **(E)** Downregulation of the *alpha subunit of the heterotrimeric Gs*, *Gaplhas* (*Galphas-IR*; *Gas-IR*) in PIL/CGL neurons using the broad driver *R19B09>* rescues the delay induced by *Tub-dilp8(2)*. Box plot showing pupariation time (AEL) in h of (N) larvae. As a negative control, stocks carrying either *R19B09>* or *Galphas>IR* were crossed with *w[1118]* animals. In all box-plot panels, whiskers extend to minimum to maximum value, each dot represents one individual, the vertical bars represent the median. $P < 0.001$, One-way ANOVA test. Genotypes sharing the same letter are not statistically different at $\alpha = 0.05$, Tukey's post-hoc test. Scale bars, 50 µm.

NEUROGENETIC MODULATION OF PIL/GCL ACTIVITY

PIL/GCL neuron silencing suppresses the Dilp8-dependent developmental delay

We next set out to genetically test whether another critical assumption of the model is also correct: that Lgr3 activation by Dilp8 leads to PIL/GCL neuron activation (**Figure 1A**). Typically, neuronal activation consists of membrane depolarization followed by synaptic vesicle release at axon terminals [43]. To test if these processes are required in PIL/GCL neurons downstream of Dilp8-Lgr3 signaling, we used a neurogenetic strategy. We first hyperpolarized PIL/GCL neurons using the *PIL/GCL>* line coupled with a *UAS-FRT-stop-FRT-Kir2.1::GFP* construct [which expresses GAL4-dependent *Kir2.1::GFP* upon FLP-mediated removal of the stop cassette [44]] in the presence or not of *Tub-dilp8(3)* (a 3rd chromosome insertion of Tub-dilp8 [18]) and scored for the pupariation timing. The hypothesis was that Kir2.1-induced hyperpolarization would counteract the effects of Dilp8/Lgr3-triggered PIL/GCL neuron depolarization, thereby suppressing the delay caused by the presence of ectopic Tub-dilp8(3) expression. In agreement with our hypothesis, we found that *Tub-dilp8(3), PIL/GCL>Kir2.1::GFP* animals pupariated significantly earlier than *Tub-dilp8(3); UAS-FRT-stop-FRT-Kir2.1::GFP* controls without *PIL/GCL>* ($P < 0.05$, Tukey's *post-hoc* test) (**Figure 5A**), demonstrating that *PIL/GCL>* neuron hyperpolarization suppresses the effect that Dilp8 has on PIL/GCL neurons. These results indicate that Dilp8-dependent Lgr3 signaling in PIL/GCL neurons leads to their depolarization and that this depolarization is required for the pupariation delay.

If PIL/GCL neurons depolarize upon Lgr3 activation, as the results above suggest, then it is a fair assumption–based on typical neuronal properties–that this depolarization is followed by the release of neurotransmitter-containing vesicles at the presynaptic terminals of PIL/GCL neurons. To test this, we blocked synaptic transmission in PIL/GCL neurons using two independent neurogenetic strategies: i) synaptic vesicle exhaustion by blocking vesicle endocytosis using the temperature-sensitive dynamin mutant allele, *shibire[ts] (shi[ts])* [45], and ii) direct synaptic vesicle exocytosis blocking using the tetanus toxin light chain (TeTxLC), which inhibits vesicle-membrane fusion events by cleaving members of the synaptobrevin/vesicle-associated membrane protein family [46]. In the first strategy, animals expressing *shi[ts]* in PIL/GCL neurons using two independent constructs (*PIL/GCL>UAS-FRT-stop-FRT-shi[ts](2)* or *-shi[ts](3)* [47]) in the presence of *Tub-dilp8(3)* or *Tub-dilp8(2)*, respectively, pupariated significantly earlier than their respective control *PIL/GCL>, Tub-dilp8(2 or 3)* animals ($P < 0.05$, Tukey's *post-hoc* test) (**Figure 5B**), but also significantly later than negative controls not carrying the *Tub-dilp8(2 or 3)* constructs ($P < 0.05$, Tukey's *post-hoc* test) (**Figure 5B**). This indicated that blocking synaptic transmission in PIL/GCL neurons partially suppresses the effect that Dilp8 has on PIL/GCL neurons, similarly to the results of neuronal hyperpolarization. This finding is highly consistent with the model that synaptic transmission occurs downstream of Dilp8-Lgr3 signaling in PIL/GCL neurons. In the second strategy, *Tub-dilp8(3)* animals expressing TeTxLC in PIL/GCL neurons using a similar genetic strategy as above (*Tub-dilp8(3), PIL/GCL>UAS-FRT-stop-FRT-TeTxLC*), also pupariated significantly earlier than the positive controls expressing a mutated, inactive form of TeTxLC, TeTxLC.IMPTNT (*Tub-dilp8(3), PIL/GCL>UAS-FRT-stop-FRT-TeTxLC.IMPTNT*) or not expressing any TeTxLC version (*Tub-dilp8(3), PIL/GCL>*) ($P < 0.05$, Tukey's *post-hoc* test for both conditions) (**Figure 5C**), but again later than the negative controls not carrying the *Tub-dilp8(3)* cassette ($P < 0.05$, Tukey's *post-hoc* test for all conditions) (**Figure 5C**). These experiments demonstrate that expression of TeTxLC in PIL/GCL neurons partially rescues the Dilp8-dependent delay in pupariation timing, and are highly consistent with the *Kir2.1* and *shit[ts]* experiments described above. As the three neuronal silencing strategies rely on the same driver intersection, and in the three cases the rescue of the *Tub-dilp8(2 or 3)*-effect was partial, rather than complete, the most conservative conclusion of these experiments is that PIL/GCL-neuron depolarization and synaptic transmission are required for the Dilp8/Lgr3-dependent delay, confirming another important assumption of the model.

Interestingly, in the absence of ectopic Tub-Dilp8 expression, all neuronal silencing experiments led to small anticipations of the median time of pupariation, although this only reached statistical significance for the neuronal hyperpolarization experiments. Namely, *PIL/GCL>Kir2.1::GFP* animals pupariated slightly earlier than *PIL/GCL>* or *UAS-FRT-stop-FRT-Kir2.1::GFP* negative controls ($P < 0.05$, Tukey's *post-hoc* test) (**Figure 5A**). In contrast, the difference was not statistically significant when *shi[ts]* or *TeTxLC* were expressed in PIL/GCL neurons in the absence of *Tub-dilp8* ($P > 0.05$, Tukey's *post-hoc* test) (**Figure 5C**). Hence, it is clear that in the experimental conditions used in this study, this small effect is not robust to the different neurogenetic silencing methods. However, the absence of a statistically significant effect in the synaptic transmission manipulation experiments could be due to the relatively small effect size of this anticipation (a few hours), which might require larger sample sizes than those used in our assay. Other assay setups, such as those using larvae synchronized at the L2-L3 molt, might be more appropriate to detect such smaller effects. For instance, such assays were used to demonstrate that *Lgr3* mutation alone leads to a ~4-h anticipation of the pupariation time in control conditions (*i.e.,* in the absence of any genetic or environmental challenge) [17]. Future studies can address this interesting question, because a minor anticipation of pupariation time due to PIL/GCL neuron silencing would also be consistent with the model where PIL/GCL neuron activity prolongs the larval phase, in this case supposedly in response to endogenous Dilp8-Lgr3 signaling.

PIL/GCL neuron activation by depolarization is not sufficient to delay the onset of pupariation

According to the current model (**Figure 1A and C**) and to the neuronal silencing results described above, the neurogenetic activation of PIL/GCL neurons should or could lead to a delay in the larval-to-pupal transition, even in the absence of any endogenous or exogenous stimuli that activates the Dilp8-Lgr3 pathway. However, our enhancer bashing experiments suggested that thermogenetic PIL/GCL-neuron activation using TrpA1 was not sufficient to cause a pupariation timing delay (see *R19B09.3A>TrpA1* in **Figure 3C-D**). It could be argued that the lack of a delay could be the consequence of the simultaneous depolarization of a "delay-inhibitory neuron" present in *R19B09.3A>* cells, but not in other *R19B09.3_CRM>* fragments. Hence, it would be expected that depolarization of PIL neurons with a more specific driver effectively delays larval development. To further support these findings, we repeated the *TrpA1* thermogenetic activation experiments, but now using the same intersectional genetics strategy used for the neuronal silencing experiments–namely, by coupling *PIL/GCL>* with a *UAS-FRT-stop-FRT-TrpA1* construct [48] (*PIL/GCL>UAS-FRT-stop-FRT-TrpA1*). Importantly, *PIL/GCL>UAS-FRT-stop-FRT-TrpA1* animals also did not pupariate significantly later than controls carrying either the *PIL/GCL>* or *UAS-FRT-stop-FRT-TrpA1* cassettes alone ($P > 0.05$, Tukey's *post-hoc* test) (**Figure 5D**). Therefore, two independent techniques and drivers indicate that favoring PIL/GCL neuron depolarization via increased cation influx is not sufficient to mimic the behavioral effects of the Dilp8-dependent activation of Lgr3 in these cells. Hence, whereas the neuronal silencing experiments demonstrate that PIL/GCL neuron depolarization is necessary for the Dilp8-dependent delay in the larval-to-pupal transition, we can now conclude that PIL/GCL neuron depolarization alone is clearly not sufficient for this delay.

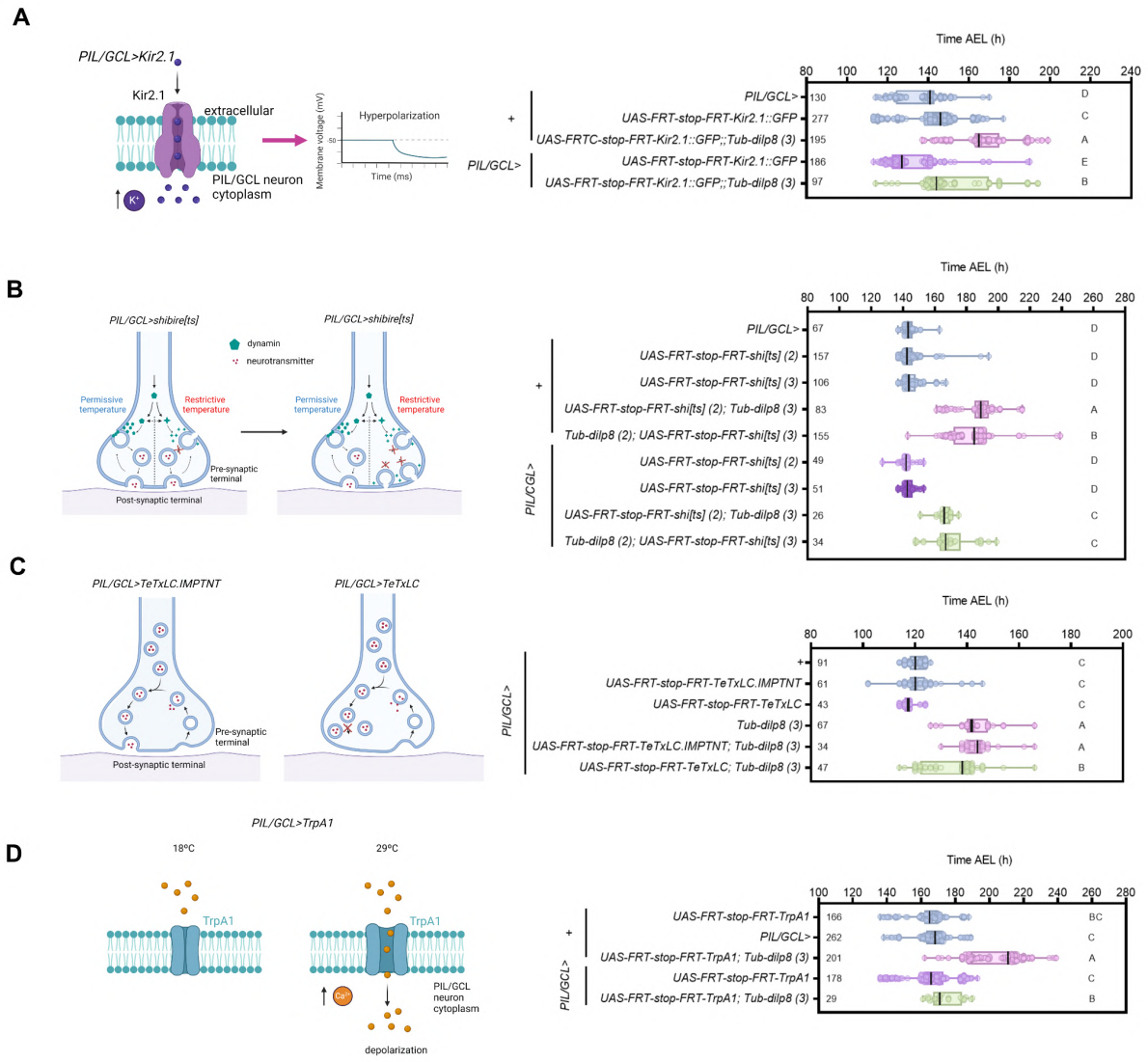

Figure 5. PIL/GCL neuron silencing or activation suppresses the Dilp8-dependent developmental delay. (A) Kir2.1-induced hyperpolarization in PIL/GCL neurons partially suppresses the delay caused by the presence of ectopic Tub-dilp8 expression. Box plot showing pupariation time (Time after egg laying (AEL)) in h of (N) larvae expressing Dilp8 under the control of Tubulin promoter [*Tub-dilp8(3)*] and *Kir.21* under control of *PIL/GCL>*. As negative controls, stocks carrying *PIL/GCL>* or *UAS-FRT-stop-FRT-Kir2.1::GFP* were crossed with *w[1118]* animals. **(B)** Inhibiting synaptic transmission by blocking vesicle endocytosis using the temperature-sensitive dynamin mutant allele *shi[ts]* in PIL/GCL neurons partially suppresses the delay caused by the presence of ectopic *Tub-dilp8* expression. Box plot showing pupariation time (AEL) in h of (N) larvae expressing Dilp8 under the control of Tubulin promoter [*Tub-dilp8(2) or (3)*] and *shi[ts]* (via constructs *UAS-FRT-stop-FRT-shi[ts](2)* or *UAS-FRT-stop-FRT-shi[ts](3)*) under control of *PIL/GCL>*. As negative controls, stocks carrying *PIL/GCL>* or either *shit[ts]* constructs were crossed with *w[1118]* animals. **(C)** Inhibiting synaptic transmission by blocking vesicle exocytosis using the tetanus toxin light chain (TeTxLC) in PIL/GCL neurons partially suppresses the delay caused by the presence of ectopic Tub-dilp8 expression. Box plot showing pupariation time (AEL) in h of (N) larvae expressing Dilp8 under the control of Tubulin promoter [*Tub-dilp8(3)*] and *TeTxLC* under control of *PIL/GCL>*. As a negative control, a stock carrying PIL/GCL> was crossed with w[1118] animals. As a positive control, a stock carrying *PIL/GCL>* was crossed with *w[1118]* animals or with animals carrying a mutated, inactive form or *TeTxLC, TeTxLC.IMPTNT*. **(D)** Thermogenetic activation of PIL/GCL neurons suppresses the Tub-dilp8 delay. Box plot showing pupariation time (AEL) in h of (N) larvae expressing Dilp8 under the control of Tubulin promoter [*Tub-dilp8(3)*] and *TrpA1* under control of PIL/GCL. As a negative control, stocks carrying *PIL/GCL>* or *UAS-FRT-stop-FRT-TrpA1* were crossed with *w[1118]* animals. In all panels, whiskers extend to minimum to maximum value, each dot represents one individual, the vertical bars represent the median. $P < 0.0001$, One-way ANOVA test. Genotypes sharing the same letter are not statistically different at $\alpha = 0.05$, Tukey's post-hoc test.

PIL/GCL neuron activation by depolarization suppresses the Dilp8-dependent developmental delay

We next wondered if this thermogenetically-induced depolarization of PIL/GCL neurons would increase the developmental delay effect in sensitized animals, which already carry a delay-inducing *Tub-dilp8(3)* cassette, and thus supposedly have activated Lgr3 signaling in PIL/GCL neurons. We

found that thermogenetic activation of PIL/GCL neurons did not further extend the Dilp8-dependent delay (**Figure 5D**) but, to our surprise, it suppressed it ($P < 0.05$, Tukey's *post-hoc* test against *UAS-FRT-stop-FRT-TrpA1*; *Tub-dilp8(3)* animals), back to the levels of *PIL/GCL>* controls ($P > 0.05$, Tukey's *post-hoc* test). The simplest interpretation of these results is that neuronal silencing is also necessary for the Dilp8-dependent delay in pupariation. Hence, apart from rejecting the current PIL/GCL functional model (**Figure 1A and C**), as described above, these results further suggested that Dilp8 activation of Lgr3 in PIL/GCL neurons is partially inhibitory, instead of only excitatory, and that this inhibition can be counteracted by cation influx to the PIL/GCL to significantly anticipate pupariation timing [17]. An alternative explanation for the TrpA1 effect would be that chronic TrpA1 activation negatively interferes with some critical function of PIL/GCL neurons, reducing their activity instead of activating them. While it is difficult to exclude this possibility completely, we believe this is unlikely to be the case for PIL/GCL neurons for three main reasons. First, temperature-dependent TrpA1 activation in larval neurons (for instance, motor neurons or serotonergic neurons) has been shown to increase neuronal activity as expected and in the case of motor neurons drive tonic action potentials with little adaptation [34-38]. Second, whereas TrpA1 is constitutively expressed in the PIL/GCL neurons, it is only activated by the temperature shift at the end of L2/beginning of L3 stage, so the time period is relatively short - even more so if one considers that the sensitive time for Dilp8 activity and hence PIL/GCL neuron activity is thought to occur most prominently at the first half of the 3rd instar larval phase before the mid-third instar transition [10,12,17]. Third, circuit architecture is mostly stable throughout the larval stages [49], so that primary neurons, such as PIL/GCL neurons, are expected to establish their connections by the L1 stage, maintaining their overall shape and connectivity up to pupariation. To confirm this is the case for PIL/GCL neurons, we studied their neuroanatomy by direct immunofluorescence observation during development using the *R19B09.3D>* driver, and found no obvious difference in gross PIL/GCL neuron morphology from L1 to Late L3 (**Supplementary Figure S2**). Hence, TrpA1 activation at late L2 and early L3 is not expected to interfere with PIL/GCL neuron growth or synaptogenesis.

How can the same pair of bilateral neurons require both silent and active phases to exert its biological effects? These apparently opposing results can be reconciled in a model where the activation of Lgr3 by Dilp8 in PIL/GCL neurons leads to oscillations in membrane potential, such that PIL/GCL neurons start transitioning between depolarized and hyperpolarized states. Such phenomena can arise by two main mechanisms, via neurons with intrinsic oscillating properties, the so-called pacemaker or pacemaker-like neurons, or via simple feedback inhibition circuits from neurons which do not have intrinsic bursting properties (reviewed in [26-27]. In the case of PIL/GCL neurons, the neurons would acquire such activity following Lgr3 activation by Dilp8. In a model where PIL/GCL neurons acquire intrinsic pacemaker activity upon Lgr3 activation, this would be analogous to how neurons in the rodent developing superficial dorsal horn neurons and adult deep dorsal horn neurons, for instance, switch between pacemaker and non-pacemaker activity upon stimulation by different factors [50-51], in the later case due to G-protein coupled receptor-dependent activation of inward-rectifying potassium (Kir) conductance [50]. Similarly, oxytocin/vasopressin-related neuropeptides have long been known to induce bursting pacemaker currents in mollusk neurosecretory and central neurons [52-53]. Alternatively, in a model where PIL/GCL neurons do not acquire intrinsic pacemaker activity, they could acquire oscillatory behavior via the Lgr3-dependent network property changes, such as by synaptogenesis, for instance, or any other mechanism that activates reciprocally inhibitory synapses between themselves and confer the circuit the potential for feedback inhibition [27].

INTRINSIC AND NETWORK PROPERTIES OF PIL/GCL NEURONS

PIL/GCL neurons express Cyclin A, a cell cycle protein involved in sleep time regulation in postmitotic neurons

To start gaining insight into PIL/GCL neuron responses, we first tested whether PIL/GCL neurons were involved in the circadian pacemaker pathway, which controls many self-sustained rhythms in physiology and behavior with ~24 h periodicity [54]. L3 larvae contain 6-8 clock neurons, which are positive for the gene *period* (*per*) [55], a product of the transcription factors Clock and Cycle (reviewed in [56]. Even though the localization of PIL/GCL neurons is not totally consistent with that of known clock neurons, we tested whether *Lgr3* would be required in *per*-positive cells, by knocking out *Lgr3* in *per-GAL4* cells [57] (*per>Lgr3-IR*) and asking if this would suppress the *Tub-dilp8* delay. If yes, this would mean that PIL/GCL neurons are clock neurons. Our results were clearly negative, showing that *Lgr3* is not required in *per>*-positive cells, indicating that PIL/GCL neurons are not clock neurons (**Figure 6A**). The neuropeptide pigment-dispersing factor (Pdf) is expressed in a subset of clock neurons [58], and is a major regulator of neuronal clock output, by modulating Pdf receptor (Pdfr)-positive cells [59]. If PIL/GCL neurons could be entrained by PDF, they would be Pdfr-positive. Hence, we tested this by knocking-down *Lgr3* in *Pdfr(B)-GAL4* cells [60] (*Pdfr>Lgr3-IR*) and asking if this was sufficient to rescue the *Tub-dilp8*-dependent delay in development. Again, our results were negative (**Figure 6A)**, showing that *Lgr3* is not necessary in *Pdfr>*-positive cells for the developmental stability pathway, indicating that PIL/GCL neurons are not likely not directly Pdf-responsive, or directly entrained by the clock neurons. Hence, it is likely that PIL/GCL neurons utilize other mechanisms of rhythmicity.

Cyclin A (CycA), which is widely known for its role in cell cycle regulation [61-62], has also been found to be expressed in postmitotic neurons in adult flies, where it functions in a dedicated pathway to determine sleep length [24]. Adult CycA-positive neurons are frequently, but not always, intermingled with circadian pacemaker neurons in the adult brain. However, the sleep promoting function of CycA, and of other players in the same pathway [namely, Regulator of Cyclin A1 (Rca1) and TARANIS (TARA), which are *Drosophila* homologs of the mammalian early mitotic inhibitor (Emi1) and the Trip-Br (SERTAD) family of transcriptional coregulators respectively] are independent of the circadian system [24- 25]. To test whether PIL/GCL neurons are involved in a similar pathway, we stained larval CNS preparations from *sfGFP::Lgr3* animals with an antibody against full length *Drosophila* CycA. As expected, CycA stains several cycling cells in the larval brain , including neuroblasts, their lineages, and inner and outer proliferating centers in the optic lobes (**Figure 6B-C and Supplementary Figure S3**). To our surprise, we found out that PIL/GCL neurons stained positive for CycA (**Figure 6D**). Another pair of Lgr3-positive neurons, the Midline Internal Lgr3-positive (MIL) neurons, required for proper progression of the pupariation motor program [62], also stained positive for CycA (**Supplementary Figure S3**). These results suggest that PIL/GCL neurons and maybe other Lgr3-positive neurons might use similar time-setting mechanisms as sleep pathway neurons. Further work is required to define the requirement of CycA in PIL/GCL neurons and how CycA, and likely the other pathway members, Rca1 and TARA, could contribute to oscillatory behaviors. Curiously, CycA can localize to synaptic terminals in adult brain neurons, opening up an exciting avenue for investigation about this CycA pathway in PIL/GCL neurons and developmental stability pathway. An alternative interpretation of this finding, which needs to be carefully ruled out in future experiments, is that CycA might be involved in endoreduplication, even though there is no evidence that PIL/GCL neurons undergo endocycles, or any other larval neuron at this stage since the brains of newly eclosed adult flies are 98–99% diploid [64].

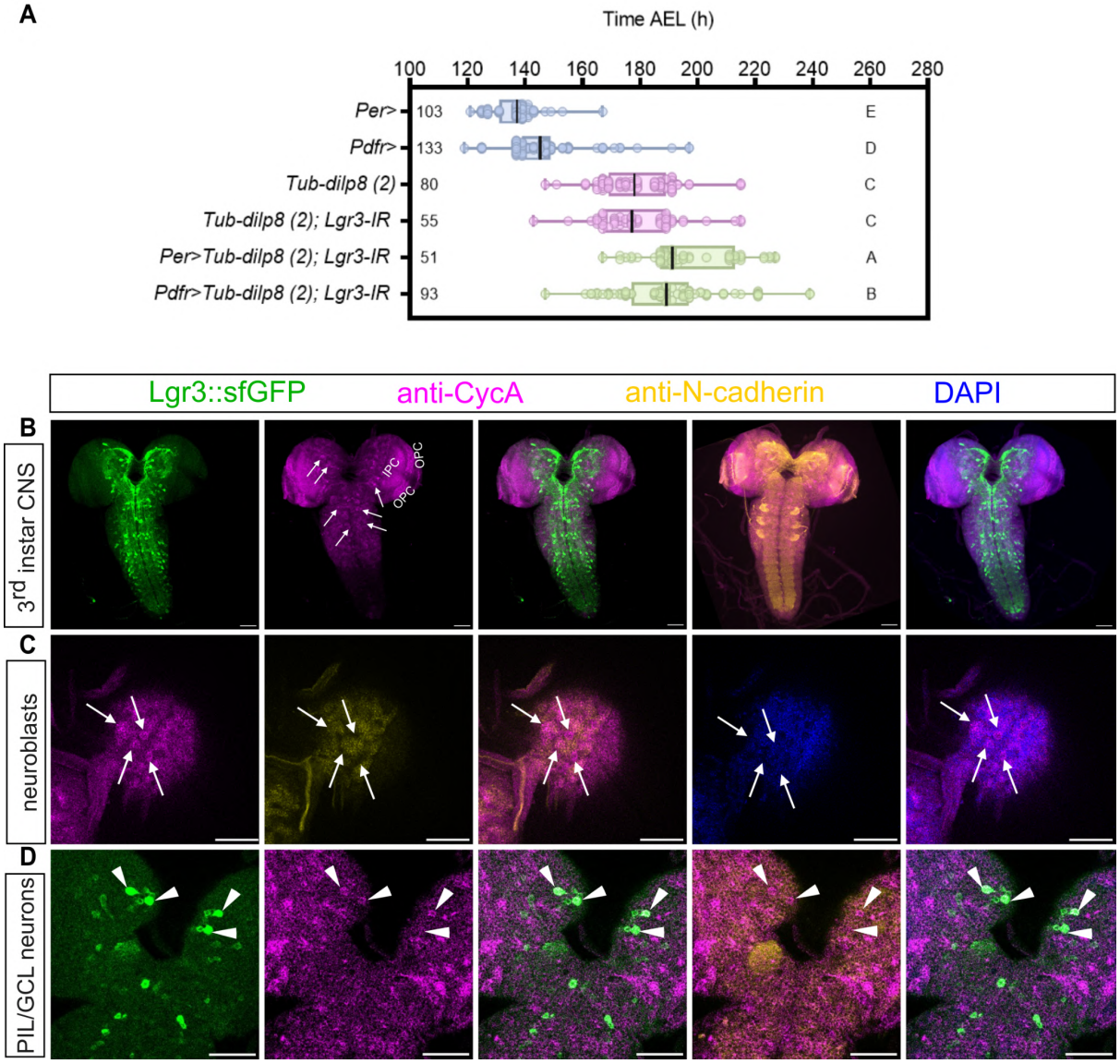

Figure 6. Lgr3 is not required in circadian pacemaker cells, and PIL/GCL neurons are CycA positive. (A) Downregulation of the *Lgr3* (*Lgr3-IR*) in *Per>* or *Pdfr>* cells does not rescue the delay induced by *Tub-dilp8(2)*. Box plot showing pupariation time (Time after egg laying (AEL)) in h of (N) larvae. As negative controls, stocks carrying either *Per>* or *Pdfr>* were crossed with *w[1118]* animals. Whiskers extend to minimum to maximum value, each dot represents one individual, the vertical bars represent the median. $P < 0.001$, One-way ANOVA test. Genotypes sharing the same letter are not statistically different at $\alpha = 0.05$, Tukey's post-hoc test. Scale bars, 50 µm. **(B)** General pattern of CycA-positive cells in the 3rd instar larva CNS. Inner (IOC) and outer (OPC) proliferative centers and several neuroblast/lineages (arrows) are visible in the magenta channel (anti-CycA). Depicted is the sum of confocal z-stack slices of an immunohistochemistry preparation obtained from a dissected 3rd instar larva CNS stained with anti-GFP (sfGFP::Lgr3, green), anti-CycA (magenta), anti-DN-Ex#8-s (anti-N-cadherin) (neuroanatomical reference, yellow), and counterstained with DAPI (nuclei, blue). Arrowheads label PIL/GCL neurons. **(C)** Same as (B) yet with less slices per projection and focusing on the superficial optic lobe area to depict neuroblasts positively stained for CycA (arrowheads). **(D)** Same as (B) but showing the *pars intercerebralis* region and four PIL/GCL neurons (arrowheads, green), of which three are clearly positive for CycA (magenta). Scale bar, 50 µm.

PIL/GCL neurons consist of two distinct neurons, a local (PIL/GCL-LN) and a projection (PIL/GCL-PN) neuron

Rhythmically oscillating neuronal networks can arise from either intrinsic properties or network properties (reviewed in [26-27]). To start gaining insight into possible network properties of the PIL/GCL neurons, we first characterized PIL/GCL neuron neuroanatomy in more detail using MultiColor FlpOut (MCFO) [65] to stochastically label *R19B09.3D>*-positive neurons, which include the PIL/GCL neurons (**Figure 7A-C**). Briefly, the MCFO strategy used (*R19B09.3D>MCFO*) included,

in addition to the *R19B09.3D>*, a panneuronally-driven FLPL (*R57C10-FLPL*), and a series of UAS- and FLPL-dependent reporters (*10xUAS(FRT.stop)myr::smGFP-HA, 10xUAS(FRT.stop)myr::smGFP-V5, 10xUAS(FRT.stop)myr::smGFP-FLAG*), which we detected using an anti-V5 antibody and an anti-sfGFP antibody [which labels smGFP ("spaguetti-monster GFP") in all *R19B09.3D>*-positive FlpOut clones]. We consistently found clones with two different branching patterns originating from cell bodies placed in the PIL/GCL neuron region (anterior/rostral-medial region of the CNS). Namely, while both PIL/GCL neurons send bilateral (both ipsilateral and contralateral) anterior projections (labeled with asterisks) to the same neuropil compartments–crossing the midline only once–, only one PIL/GCL neuron from each hemibrain has an additional ipsilateral descending projection to the SEZ, as can be seen in the **Figures 7A-C** (asterisk). This latter PIL/GCL neuron can be classified both as a projection neuron (PN, which are interneurons that carry information between brain regions; following the classification of [66], which does not distinguish between first-hop PNs and output neurons) and also a descending neuron towards the SEZ (DN-SEZ). We named this neuron PIL/GCL-PN. The other PIL/GCL neuron has a branching pattern consistent with a local neuron (LN), defined as a neuron that processes information within a single neuropil compartment (ipsilaterally, contralaterally, or bilaterally). Hence, we called this neuron, PIL/GCL-LN. PIL/GCL-LNs are most likely of the bilateral type (**Figure 7A**), which would make it one of the eight known bilateral LNs in the larval brain [66]. This should facilitate their identification in the reconstituted L1 electron microscopy data for further connectomic studies.

Other brain neurons were also labeled by *R19B09.3D>MCFO*, albeit less frequently, including one or more neurons, which we believe could be other #5 neurons, with cell bodies localized in the same anatomical region as the PIL/GCL neurons cell bodies (**Figure 7C, arrow**), and another more posterior neuron (**Supplementary Figure S4**). This neuronal type projects to both sides and to the SEZ, similarly to the PIL/GCL-PN, but has a more straight/linear path in the mediolateral axis. The PIL/GCL neurons can be distinguished by their more curvilinear projections to a more anterior area of this neuropil compartment (**Figure 7C, green**). Whereas the full relevance of these neuroanatomical findings are not completely clear at this stage, we can already learn at least two important facts that are relevant to this study: first, the different branching patterns between PIL/GCL-LN and -PNs reveals an unforeseen layer of complexity in PIL/GCL neuron biology, suggesting specialized functions for each PIL/GCL neuron subtype, rather than a single function as previously modeled. Second, both PIL/GCL neurons (LN and PN) seem to share reciprocal bilateral projections, suggesting that they might be subject to contralateral feedback, which is a common oscillator-triggering mechanism [27].

PIL/GCL-LN and -PN neurons are bilateral and likely form reciprocal loops

To gain more insight into the directionality of information processing of PIL/GCL neurons, we first expressed a V5-tagged version of the pre-synaptic active-zone marker, Bruchpilot [67], (Brp::V5), in *R19B09 ∩ MZ699>* neurons using a similar FlpOut strategy [68]. Because of the particularities of this cross, we see Brp::V5 from all R19B09 *and* MZ699 drivers, which includes all #5 neurons. Nevertheless, we found strong Brp-labeling in the PIL/GCL neuron (and other #5 neuron) anterior projections, but no or very limited positive staining in their descending projections (**Figure 7D**). The simplest interpretation of this finding is that the descending branches of all #5 PNs, which include the PIL/GCL-PNs, are mostly, if not exclusively dendritic, as they are largely devoid of Brp staining. To independently confirm this finding, we performed specific co-labeling of PIL/GCL neurons with pre- and postsynaptic markers. Namely, we used the synaptic vesicle marker, synaptotagmin 1 (syt::GFP) (*UAS-syt.eGFP*; ref.[69]), and the somatodendritic marker, DenMark (Dendritic Marker, a hybrid protein of the mouse dendritically-targeted protein, ICAM5/Telencephalin, and mCherry; ref.[70]),

which are expected to label most clearly the PIL/GCL neuron axonal and dendritic compartments, respectively. Consistently, with the experiments described above, we found that the PIL/GCL neuron (and likely those of other neighboring #5 neurons) anterior projections are decorated strongly with syt::GFP, whereas DenMark staining was found most prominently, but not exclusively, in the soma and descending projections (**Figure 7E**). These results confirm that the anterior bilateral projections of PIL/GCL neurons (both LNs and PNs) contain their axons (and relatively less postsynaptic markers), and that the descending ipsilateral projection of the PIL/GCL-PN is mostly or exclusively dendritic. We conclude that both PIL/GCL neuron types, -LNs and -PNs, send anterior bilateral projections towards homologous compartments. The LNs (and DNs) likely transmit and receive information in this neuropil region, likely forming reciprocal contralateral loops, which are enriched in brain areas that play a role in action-selection and learning [66]. On the other hand, only the PIL/GCL-PN dendrites collect ipsilateral information from more posterior brain regions and the SEZ–a zone receiving rich sensory information input [66]. Connectomics data from electron microscopy–based reconstruction of the CNS of an L1 larva show that there are at least 566 PNs with a similar neuroanatomy in the cluster of brain neurons with ipsilateral dendrites and bilateral axons [66]. Only a subset of these have cell body localizations and branching patterns consistent with PIL/GCL-PNs, which should facilitate their identification in the L1 connectomics dataset. A model summarizing the neuroanatomical results for each PIL/GCL neuron is described in **Figure 7F**.

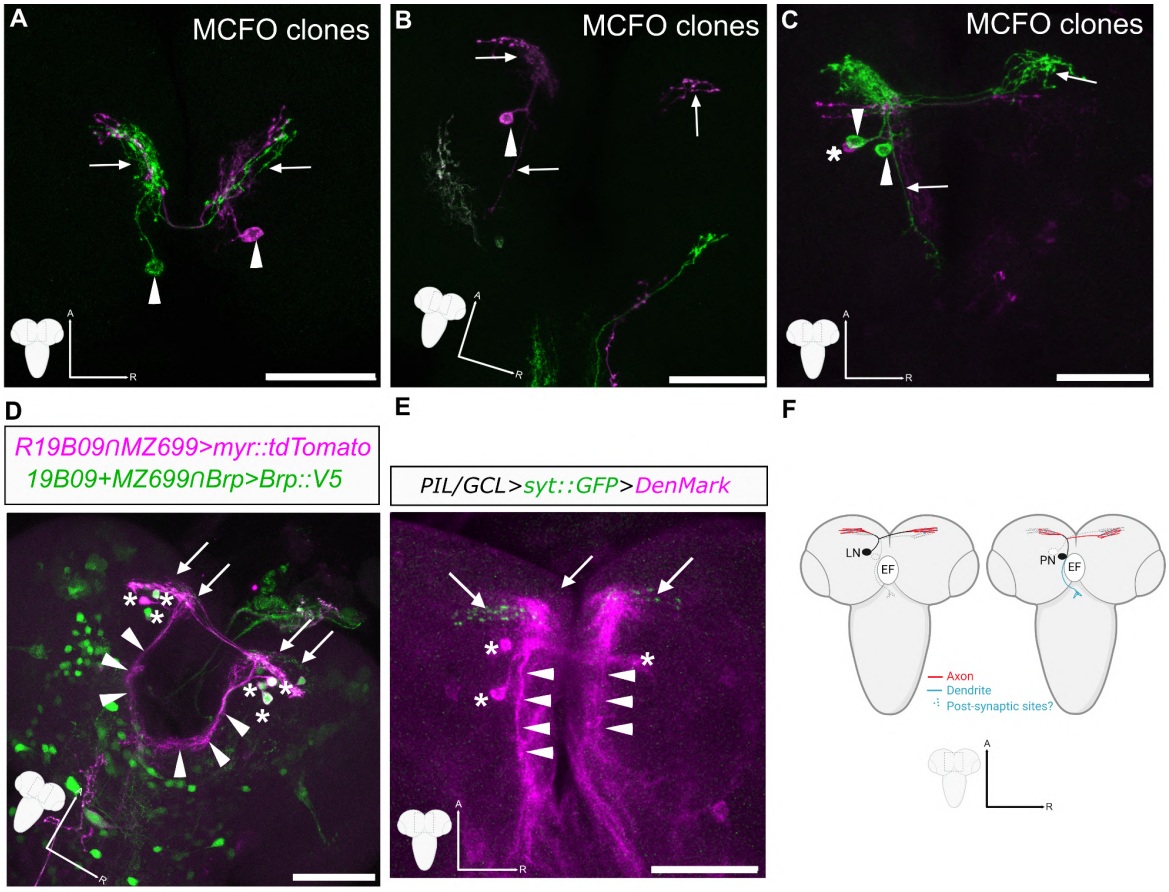

Figure 7. PIL/GCL neuroanatomy and new model for the role of PIL/GCL neurons in the Dilp8-Lgr3 developmental stability pathway. (A-C) Sum of confocal z-stack slices of MCFO labeling of L3 larval stage neurons with panneuronally (*R57C10>*)-driven expression of *FLP* and *R19B09.3D>*-driven expression *UAS*-driven MCFO markers differentially labeled here with anti-GFP (green) and anti-V5 (magenta). Arrowheads highlight PIL/GCL neuron cell bodies. Arrows label PIL/GCL neurons projections. Asterisks highlight PIL/GCL neuron closer cells. **(A)** Two MCFO clones showing two apparently homologous PIL/GCL local neurons (PIL/GCL-LNs, magenta and green). Both PIL/GCL-LNs have proximal ipsilateral and distal contralateral projections, which arborize to the same neuropil compartments, likely making reciprocal connections, which would make them one of the eight described bilateral LNs [65]. **(B)** A single PIL/GCL projection neuron

(PIL/GCL-PN) clone (magenta). This neuron has similar ipsilateral and contralateral projections to the PIL/GCL-LNs depicted in (A), but in addition, has a descending projection towards the SEZ. **(C)** Two ipsilaterally-localized PIL/GCL neuron clones are labeled in green, but only a single green-labeled projection descends towards the SEZ. Hence, these two PIL/GCL neurons represent a PIL/GCL-LN and a PIL/GCL-PN. Another neighboring #5 neuron (magenta), which has a different pattern of ipsi- and contralateral projections (more posterior and straight) than those of PIL/GCL neurons is also visible in this image. It also has a descending projection towards the SEZ. **(D)** Presynaptic sites of #5 neurons, a group of neurons which include the PIL/GCL neurons, are almost exclusively located in the anterior bilateral projections. Shown is the sum of confocal z-stack slices of dissected wandering L3 larval stage CNSs stained with anti-GFP (green). In this preparation, ***R19B09 ∩ MZ699>*** drives expression of *myr::tdTomato* (magenta) and *R19B09>>* and *MZ699>* also independently drive the expression of *brp*-driven (neuronally-driven) Brp::V5 (detected with an anti-V5 antibody, green) in R19B09+brp- or MZ699+brp-positive neurons, respectively. This is possible as in this cross there is a *8xLexAop2-FLPL* and a *UAS-FLP* cassette, which can mediate FRT removal of the *brp-FRT-stop-FRT-V5* cassette. Hence, all *MZ699>*-positive #5 neurons are labeled. Their cell bodies are highlighted with asterisks. Anteriormost projections corresponding to PIL/GCL neurons are labeled with arrows. Descending projections are labeled with arrowheads. **(E)** Dendritic and axonal compartments of PIL/GCL neurons labeled with somatodendritic marker, DenMark (magenta), and the synaptic vesicle marker, syt::GFP (green), respectively. PIL/GCL neuron (and possibly other #5 neuron) cell bodies (asterisks), axonal compartments (arrows), and dendritic compartments (arrowheads) are depicted. Notice the absence of syt::GFP in the descending projections, indicating they are mostly, if not exclusively enriched for postsynaptic sites (dendritic). A full CNS confocal projection of this preparation is depicted in **Supplementary Figure S5**. **(F)** Model describing PIL/GCL neuron neuroanatomy. Circles represent the cell body of each PIL/GCL neuron (PIL/GCL-LN and -PN, for local and projection neuron, respectively), which send bilateral anterior projections to the homologous neuropil compartments. Only PIL/GCL-PN also sends a descending projection to the subesophageal zone (SEZ), localized below the esophageal foramen (EF). Projections are colored to depict the axonal (red) and dendritic (blue) compartments of both cell types. We hypothesize that the anterior projections of both PIL/GCL-LNs and -PNs are bilateral in nature, with bilateral presynaptic and postsynaptic sites, but this remains to be formally tested with connectomics data. Scale bars, 50 µm.

A REVISED MODEL OF PIL/GCL NEURON ACTIVITY IN THE DEVELOPMENTAL STABILITY PATHWAY

PIL/GCL neurons as a model for hypothalamic-like multimodal integration

While further work is required to match PIL/GCL neuron FlpOut-clone neuroanatomy to the reconstructed electron microscopy synaptic-level pattern, which is critical to describe the full list of its upstream and downstream circuit components, our findings nevertheless open up the possibility that one of the functions of PIL/GCL neurons is to integrate SEZ-derived primary sensory inputs with the endocrine tissue-damage Dilp8 signal, to temporarily block the progression of pupariation and promote developmental stability. PIL/GCL neurons are therefore in a privileged position to integrate external and internal state information, which is the basis of encoding adaptive behavior [71]. Interestingly, such integration, which is similar in concept to neuronal binding (*i.e.,* how items encoded in distinct brain circuits or neural populations can be combined for perception, decisions, and actions [72]), is one of the functions proposed for oscillatory neurons or circuits [72-75]. PIL/GCL neurons are also localized in a fly brain region orthologous to the mammalian hypothalamus [76], which performs similar multimodal integrations of sensory, metabolic, visceral, and hormonal signals, being a key brain center modulating transitions in innate behaviors and states, many times via changes in oscillatory behavior of hypothalamic neurons [26,77-80]. For example, certain hypothalamic neurons possess a hyperpolarization-activated current, the h-current (also termed the 'pacemaker current'), which also produces the heart beat [81]. It will be interesting to verify if PIL/GCL neurons also possess such properties. Whereas we present neurogenetic and neuroanatomical evidence consistent with oscillatory behavior, one limitation of our study is that in the absence of neurophysiological observations, it is unclear what type of oscillatory behavior these neurons would acquire upon Dilp8 stimulation and for how long they maintain it. As discussed above, our data could be explained either by intrinsic or network properties. But also, within the realm of intrinsic properties, pacemaker-like neurons can have wildly different intrinsic membrane properties, such as endogenous bursting and plateau potentials, which originate in bistable neurons that enter and leave a plateau when receiving a depolarization and

hyperpolarization pulse, respectively [82]. Our findings for PIL/GCL would be consistent with either type of intrinsic membrane property.

PIL/GCL neurons as a model for neuropeptide-activated oscillatory behavior in higher brain areas

As mentioned above, the neuroanatomy of PIL/GCL neurons is consistent with that of other spontaneously oscillating circuits. This is most notable for certain central pattern generators, whose rhythmicities are well-known to be activated, modified, and terminated by neuromodulators [27], but also of other rhythmically-active neuronal networks generating non-rhythmic behaviors, such as sleep, arousal, and other higher brain functions (reviewed in [26]). The oscillating hypothalamic neurons described above, for instance, are affected by the sleep-modulating peptide, cortistatin [81]. Therefore, our key finding that Dilp8 triggers both depolarized and hyperpolarized states in PIL/GCL neurons is likely of broad relevance and can serve as a model for studying these responses in higher brain circuits. It is also relevant that our work points to an involvement of the Dilp8-Lgr3 relaxin-like pathway in the control of rhythmically active neuronal networks. Interestingly, in vertebrates, a Dilp8 orthologue, relaxin 3, and its receptor [relaxin-family peptide receptor 3 (RXFP3)] in the medial septum complex are involved in oscillatory brain activity at the theta frequency in the rat hippocampus [83-84], suggesting that our findings can also be relevant to relaxin-mediated signaling in other organisms and systems.

PIL/GCL neurons as a new model to study the role of Cyclin A in postmitotic neurons

Surprisingly, we find that PIL/GCL neurons stain positive for Cyclin A (CycA), which has previously been implicated in regulating sleep amount together with other proteins Rca1 and TARA, all in close connection with—but independently of—circadian pacemaker cells, providing a first hint towards a possible rhythm-control pathway [24]. However, how this pathway regulates sleep rhythms is not fully understood. Further work directed to dissecting a possible role for CycA in PIL/GCL neurons and how it relates to the network properties of the PIL/GCL neurons described above could possibly shed light not only into the mechanisms of the oscillatory response of PIL/GCL neurons to the Dilp8-dependent Lgr3 activation, but also to sleep rhythm regulation. The fact that both the adult CycA-positive neurons and the larval PIL/GCL-CycA positive neurons occupy similar brain areas (*pars lateralis* and *intercerebralis*) [17,24-25], which are orthologous to the mammalian hypothalamus, support the relevance of this hypothesis. Hence, the new model that arises from our work (**Figure 8**), where Dilp8 induces PIL/GCL neuron oscillatory responses, and that these are critical for the behavioral change (delay in pupariation behavior) that promotes developmental stability, is both consistent with the intrinsic and neuroanatomical properties of PIL/GCL neurons and the physiological expectations of neurons with such properties.

Implication of the model to the Dilp8-Lgr3 developmental stability pathway. PIL/GCL neurons as regulators of downstream oscillations?

Here we have tested the initial aspects of a model of the Dilp8-Lgr3 pathway, confirming the initial predictions of the model, which had not yet been subject to specific genetic testing. Specifically, we have confirmed the role of *Lgr3* in PIL/GCL neurons, and the role of stimulatory G_s in the Dilp8-Lgr3 pathway, even though we could not show this latter requirement with the same specificity as we achieved for *Lgr3* due to technical reasons. These results are consistent with Lgr3 using Galphas

signaling to increase cAMP levels via adenyl cyclase, and explains previous results using CRE-reporters and confirms the assumptions therein [17-18]. A connection between Galphas signaling, cAMP increase, and downstream activities remains to be made.

We then made the surprising observation that both depolarized and hyperpolarized PIL/GCL neuron states are required for their proper response to ectopic Dilp8 activity. This led to the proposition of a new model where PIL/GCL neurons respond to Dilp8 by becoming oscillators or becoming part of an oscillating circuit (**Figure 8**). The next neurons in this developmental stability neuroendocrine circuit are thought to be the PTTH neurons. Larval PTTH neurons integrate many developmental and environmental signals, receiving input from different neuronal pathways, so that their regulation is complex [85-87]. PTTH neurons have the important function of producing and secreting PTTH [and other factors, such as the The Alk ligand Jelly belly (Jeb)], onto the prothoracic gland, which together contribute to the timely triggering of ecdysone biosynthesis [85,87-89]. The function of PIL/GCL neurons—when activated by Dilp8-Lgr3—would be to inhibit PTTH neuron function, thereby delaying the biosynthesis of ecdysone and consequently inhibiting developmental timing progression and the growth of imaginal discs in parallel [1-4,10]. Many questions arise from our work. For instance, how does Lgr3-Galphas-cAMP-signaling in PIL/GCL neurons mediate signaling to the PTTH-producing neurons, especially in the context of PIL/GCL neuron oscillation (**Figure 8**)? What would be the impact of such oscillations on PTTH neuron function? Curiously, *PTTH* mRNA transcription shows an unusual cyclic pattern with an ~8-h periodicity throughout the larval growth stage before the mRNA levels increase several fold as the larva approaches pupariation time [88]. Hence, oscillatory *PTTH* mRNA production is a characteristic of the larval growth stage. *PTTH* mRNA levels and their periodicity are controlled by the circadian pathway during this stage, albeit only partially [88]. Namely, *PTTH* mRNA production still oscillates with an increased period in *Pdf* mutants, suggesting that other mechanisms contribute to this oscillation. As the Dilp8-Lgr3 signaling pathway and PIL/GCL neurons are considered to act upstream of PTTH neurons and *PTTH* mRNA production in the developmental stability pathway [8-9,16,18,90], it is tempting to speculate that PIL/GCL neurons are instructive to this *Pdf*-independent mRNA oscillation, promoting and prolonging the early 3rd instar larval stage-like oscillations, thus counteracting the surge of *PTTH* at the end of the larval phase. In support for this hypothesis is the fact that endogenous *dilp8* mRNA production fluctuates during the 3rd instar larval stage in the absence of abnormal growth [9]. *dilp8* mRNA levels are over an order of magnitude lower under normal conditions than when there is imaginal disc abnormal growth (*e.g.,* [8-9]), but the mRNA levels are higher in earlier 3rd instar larvae than in latter stages [9] This early Dilp8 production could theoretically lead to a developmentally-triggered Lgr3 activation in PIL/GCL neurons in early 3rd instar larvae, which could trigger PIL/GCL neuron oscillations, and hence contribute to the generation of the characteristic low level *PTTH* mRNA oscillation of earlier stages. This would also be consistent with previously proposed endogenous functions of the Dilp8-Lgr3 pathway, as revealed by anticipations of pupariation time in *dilp8* and *Lgr3* mutants in the absence of any genetic or environmental challenges, which implies that *PTTH* surges occurred precociously in these mutants [8-9,17].

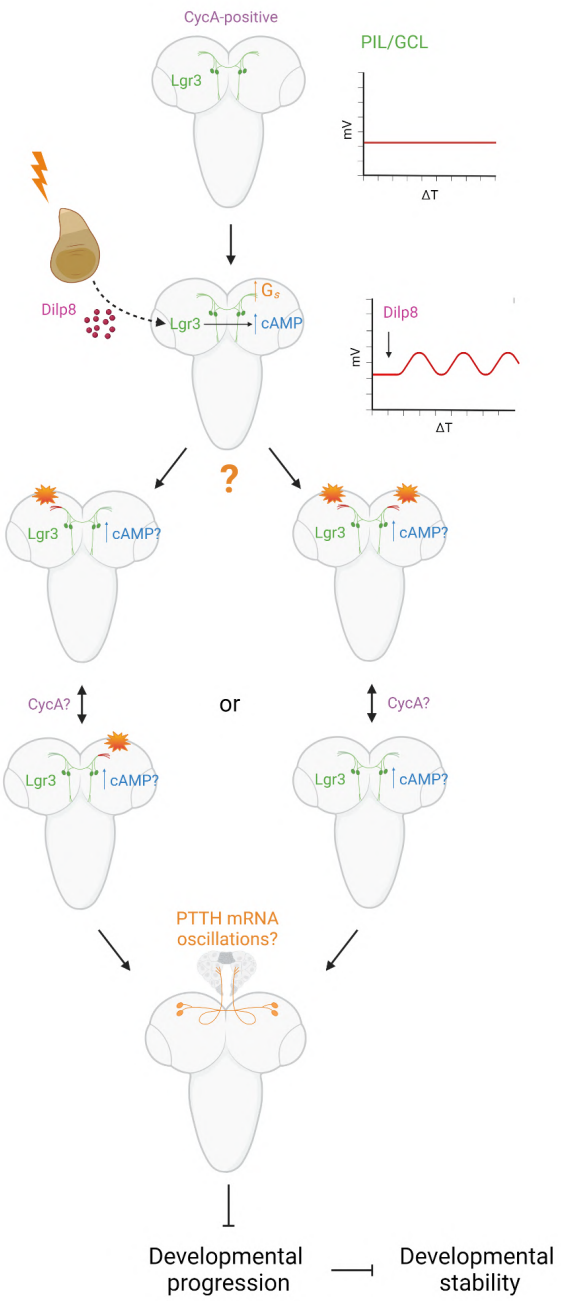

Figure 8. A new model for the role of PIL/GCL neurons in the Dilp8-Lgr3 developmental stability pathway. Upon imaginal disc damage (orange ray), imaginal disc cell abnormal growth triggers Dilp8 production and secretion (dark magenta circles), which activates Lgr3 in PIL/GCL neurons (green neurons). Lgr3 activity requires stimulatory G protein (G_s, orange), which leads to an increase in cAMP levels (blue), and both depolarized and hyperpolarized states (oscillations in membrane potential, red curves in graphs, and orange flairs in the PIL/GCL neuron axons in the CNS schemes), which are required for the inhibition of the larval-to-pupal transition, which promotes developmental stability. In this model, it is unclear whether the oscillations occur contralaterally (left branch of the model) or bilaterally (right branch of the model), as well as their period. It also remains to be determined if oscillations arise from intrinsic pacemaker-like activity of PIL/GCL triggered by the Dilp8-Lgr3-G_s-cAMP pathway (namely, that PIL/GCL neurons would oscillate even in isolation upon Lgr3 activation), or whether activation of this pathway leads to oscillations due to circuit architecture properties (feedback loops), which would mean that PIL/GCL neurons would only oscillate within their circuit context, not in isolation. The neuroanatomy of PIL/GCL neurons, a couple of bilateral local and projection neurons with a potential to form reciprocal pair loops, leads us to favor the latter model (right). The Dilp8/Lgr3 pathway and PIL/GCL neurons are proposed to act upstream of PTTH neurons (not experimentally addressed in this manuscript), which show oscillating production of *PTTH* mRNA in early 3rd instar larval periods. A tempting hypothesis is that endogenous Dilp8-Lgr3 promoted PIL/GCL neuron oscillations partially contribute to such *PTTH* mRNA oscillations during normal development and, in the presence of abnormal imaginal disc growth, the persistent Dilp8-Lgr3 signaling perpetuates this early-stage oscillatory pattern via prolonged PIL/GCL neuron oscillation, delaying the larval-to-pupal transition and promoting developmental stability.

MATERIALS AND METHODS

Drosophila husbandry and stocks

The stocks were reared in standard *Drosophila* food, and kept at 18ºC, ~60%RH, 12-h light/dark cycle. All experiments were performed at 25ºC, 12-h light/dark cycle.

sfGFP::Lgr3^{ag5} was previously described [17]. *tsh-Gal80/CyO* (*r*ef.[41]) was a gift from Carlos Ribeiro. *w[1118]* and *Tub-dilp8(2)* and *(3)*, corresponding to 2nd and 3rd Chr insertions, respectively (ref.[18]), were gifts from Maria Dominguez. *MZ699-GAL4* (ref.[21]), *UAS-FRT>CD2>FRT-Kir2.1-GFP* (*UAS-FRT-stop-FRT-Kir2.1::GFP*) (ref.[44]), BL28842 w[*]; P{UAS(FRT.w[+mW.hs])TeTxLC}10/CyO (*UAS-FRT-stop-FRT-TeTxLC*) (ref.[47]), *BL28843* w[*]; P{UAS(FRT.w[+mW.hs])TeTxLC.IMPTNT}14A *UAS-FRT-stop-FRT-TeTxLC.IMPTNT*) (ref.[47]), and *w; UAS>stop>TrpA1/CyO* (*UAS-FRT-stop-FRT-TrpA1*) (ref.[48]) were gifts from Maria Luisa Vasconcelos and Marta Aranha. *UAS-TRPA1/CyO* was a gift from Christen Mirth. *w;;GMR19B09.1.1-GAL4, w;;GMR19B09.2.1-GAL4, w;;GMR19B09.3.1-GAL4, w;;GMR19B09.3A.1-GAL4, w;;GMR19B09.3B.1-GAL4, w;;GMR19B09.3C.1-GAL4, w;;GMR19B09.3D.1-GAL4,* and *w;;GMR19B09.3E.1-GAL4* (ref.[29]) were gifts from Geoffrey Meissner and Bruce Baker.

The following lines were obtained from the Bloomington Drosophila Stock Center at Indiana University:

BL36887 *y[1] sc[*] v[1] sev[21]; P{y[+t7.7] v[+t1.8]=TRiP.GL01056}attP2/TM3, Sb[1] (UAS-Lgr3-IR-V22)* (ref.[30])

BL48840 *w[1118]; P{y[+t7.7] w[+mC]=GMR19B09-GAL4}attP2* (ref.[28])

BL32222 *w[*]; P{y[+t7.7] w[+mC]=10XUAS-IVS-myr::tdTomato}attP40* (ref.[31])

BL32219 *w*; P{10XUAS-IVS-mCD8::RFP}attP40* (ref.[31])

BL55810 *w[1118]; P{y[+t7.7] w[+mC]=10XUAS(FRT.stop)GFP.Myr}su(Hw)attP5* (*UAS-FRT-stop-FRT-GFP*) (ref.[39])

BL38879 *P{w[+mC]=alphaTub84B(FRT.GAL80)}1, w[*]; Bl[1]/CyO; TM2/TM6B, Tb[1]* (ref.[40])

BL55819 *w[1118]; P{y[+t7.7] w[+mC]=8XLexAop2-FLPL}attP2* (ref.[31])

BL66675 *w[*]; P{w[+mC]=UAS(FRT.stop)shi[ts]}2* (ref.[47])

BL66676 *w[*]; P{w[+mC]=UAS(FRT.stop)shi[ts]}3* (ref.[47])

BL33064 *w1118; P{UAS-DenMark}2, P{UAS-syt.eGFP}2; In(3L)D, mirrSaiD1 D1/TM6C, Sb1* (ref.[70])

BL64089 *w[1118] P{y[+t7.7] w[+mC]=R57C10-FLPG5.PEST}su(Hw)attP8; PBac{y[+mDint2] w[+mC]=10xUAS(FRT.stop)myr::smGdP-HA}VK00005 P{y[+t7.7]*

w[+mC]=10xUAS(FRT.stop)myr::smGdP-V5-THS-10xUAS(FRT.stop)myr::smGdP-FLAG}su(Hw)attP1 (ref.[65])

BL55752 *w[*]; P{y[+t7.7] w[+mC]=LexAop-tdTomato.Myr}su(Hw)attP5; P{w[+mC]=UAS-FLP.D}JD2, PBac{y[+mDint2] w[+mC]=brp(FRT.Stop)V5-2A-LexA-VP16}VK00033* (ref.[91])

BL682125 *w[*]; P{w[+mC]=Pdfr-GAL4.B}2/CyO* (ref.[60])

BL7127 *y[1] w[*]; P{w[+mC]=GAL4-per.BS}3* (ref.[57])

BL 50704 *y[1] v[1]; P{y[+t7.7] v[+t1.8]=TRiP.HMC03106}attP2* (*UAS-Galphas-IR*) (ref.[30])

The stocks were reared in standard *Drosophila* food, and kept at 18ºC, ~60%RH, 12-h light/dark cycle. All experiments were performed at 25ºC, 12-h light/dark cycle.

Immunofluorescence analyses

CNS of larvae L3 wandering were dissected in Schneider Medium (Biowest – cat. #L0207 or Gibco - cat. #21720-024), fixed for 30 min in 4% paraformaldehyde, rinsed with PBS with Triton (0.3%) (PBST), incubated with primary antibody for 24-48h and with fluorescently labeled secondary antibody for 2–24 h in PBST with 1% bovine serum albumin. Samples were washed 3x for 30 min each in PBST after each antibody incubation. Nuclei were counterstained with DAPI (Sigma) and tissues were mounted in DABCO mounting medium. Primary antibodies used were: Rabbit Anti-GFP, 1:200 (Life Technologies, A11122); Rabbit Living Colors DsRed, 1:500 (Clontech, 632496); Mouse Anti-GFP-4C9, 1:200 (DSHB, DSHB-GFP-4C9), Mouse nc82-s, 1:100 (DSHB, AB_2314866), Mouse anti Cyclin A (A12), 1:100, (DHSB, AB_528188), Rat DN-Ex #8-st, 1:50 (DSHB, AB528121). Secondary antibodies were: Alexa Fluor 488, anti-mouse (Life Technologies, A11029); Alexa Fluor 488, anti-rabbit (Life Technologies, A11070); Alexa Fluor 488, anti-rat (Invitrogen, A21208), Alexa Fluor 568, anti-rabbit (Life Technologies, A11036); Alexa Fluor 594, anti-mouse (Life Technologies, A11020), Alexa Fluor 647 anti-rabbit (Jackson Immuno Research, 711-605-152). Images were obtained with a Zeiss LSM 710 or a Leica SP5 Confocal Microscopes. Images were analyzed using FIJI software [92]. Usually, 5 to 10 CNS were mounted for observation and 1 representative image per genotype is depicted in figures. CNS from male and female larvae were scored together.

Measurement of the developmental timing of pupariation

Male and virgin female flies aged 3-15 d were crossed and 48 h later transferred to an agar plate with yeast paste. The next morning, the flies were transferred to a fresh plate to lay eggs for 2 h. The plates were exchanged every 2 h, 4-5 times a day. Second instar larvae (48 h after egg laying) were transferred to vials containing standard *Drosophila* food. To prevent overcrowding, the number of larvae per vial was between 20 to 30. Survey of pupae consists in counting the number of puparia in each time interval. The final number of pupae for each genotype in each experiment is depicted in the respective figures. For pupariation time assays, we aimed at obtaining at least 30 individual larvae per genotype, yet some genotypes were sick or difficult to obtain due to balancer chromosomes, yielding fewer larvae of the correct genotype to score. Males and females were scored together. These experiments were performed at 25±1 °C, except for experiments using flies carrying the *TrpA1* and *shi[ts]*, which were performed at

18 °C until the second instar (72 h after egg laying) after which the larvae were transferred to 29 °C to activate the system.

General study design and statistics

In all experiments reported in this work, no data point was excluded. All data points, including outliers, are represented in the figures and were used in the statistical analyses. No blinding was done and no particular randomization method was used to attribute individuals to experimental groups. Statistics were performed in RStudio (RStudio: Integrated Development for R. RStudio, PBC, Boston, MA URL http://www.rstudio.com/). Graphs were made in GraphPad Prism version 8.0.2 for Windows, GraphPad Software, Boston, Massachusetts USA, www.graphpad.com.

AUTHOR CONTRIBUTIONS

R.Z., J.P., M.F-A., M.P., A.P.C., A.G., and F.H. performed genetic, phenotypic, and behavioral experiments, and contributed to image and data analyses. F.H., A.G., and A.M.G. supervised the work. A.M.G. and A.G. contributed to image and data analyses. A.M.G. wrote the manuscript with the help of all authors.

ACKNOWLEDGEMENTS

We thank Drs. Maria Luisa Vasconcelos, Carlos Ribeiro, Christen Mirth, Maria Dominguez, Geoffrey Meissner, and Bruce Baker for fly stocks. We thank lab members for discussions and/or comments on the manuscript. Stocks obtained from the Bloomington Drosophila Stock Center (NIH P40OD018537) were used in this study. TRiP RNAi stocks were used in this study (Office of the Director R24 OD030002). The monoclonal antibodies Anti-GFP-4C9, nc82-s, anti-Cyclin A(A12), and DN-Ex #8-st developed by DSHB, E. Buchner, Christian Lehner, and T. Uemura, respectively, were obtained from the Developmental Studies Hybridoma Bank, created by the NICHD of the NIH and maintained at The University of Iowa, Department of Biology, Iowa City, IA 52242. Work in the Integrative Biomedicine Laboratory was supported by the European Commission FP7 (PCIG13-GA-2013-618847), by the FCT (PTDC/BEXBCM/1370/2014; PTDC/BIA-BID/31071/2017; PTDC/MED-NEU/30753/2017 (LISBOA-01-0145-FEDER-030753, with financing from the Programa Operacional Lisboa 2020); EXPL/BIA-BID/1524/2021; EXPL/BIA-COM/1296/2021; 10.54499/2022.03859.PTDC), by the UIDs iNOVA4Health (10.54499/UIDB/04462/2020) and cE3c (10.54499/UIDB/00329/2020), by LS4FUTURE (10.54499/LA/P/0087/2020) and CHANGE (10.54499/LA/P/0121/2020) financed by the FCT/MCTES (Portugal), and by Congento LISBOA-01-0145-FEDER-022170, co-financed by FCT/Lisboa2020; UID/Multi/04462/2019. Work in the Garelli lab was also supported by ANPCyT (Agencia Nacional para la Promoción de la Ciencia y la Tecnología, PICT 2017-0254 and PICT 2020-01568), CONICET (PIP11220150100182CO) and Universidad Nacional del Sur PGI 24/B288. AMG and FH were individually supported by grants 10.54499/CEECINST/00102/2018/CP1567/CT0031 and 10.54499/DL57/2016/CP1457/CT0016, respectively. AG is a CONICET researcher.

REFERENCES

[1] Juarez-Carreño S, Morante J, Dominguez M. Systemic signalling and local effectors in developmental stability, body symmetry, and size. Cell Stress. 2018 Nov 13;2(12):340-361. doi: 10.15698/cst2018.12.167. PMID: 31225459; PMCID: PMC6551673.

[2] Mirth CK, Shingleton AW. Coordinating Development: How Do Animals Integrate Plastic and Robust Developmental Processes? Front Cell Dev Biol. 2019 Feb 6;7:8. doi: 10.3389/fcell.2019.00008. PMID: 30788342; PMCID: PMC6372504.

[3] Texada MJ, Koyama T, Rewitz K. Regulation of Body Size and Growth Control. Genetics. 2020 Oct;216(2):269-313. doi: 10.1534/genetics.120.303095. PMID: 33023929; PMCID: PMC7536854.

[4] Boulan L, Léopold P. What determines organ size during development and regeneration? Development. 2021 Jan 11;148(1):dev196063. doi: 10.1242/dev.196063. PMID: 33431590.

[5] Harmansa S, Lecuit T. Forward and feedback control mechanisms of developmental tissue growth. Cells Dev. 2021 Dec;168:203750. doi: 10.1016/j.cdev.2021.203750. Epub 2021 Oct 2. PMID: 34610484.

[6] Hallgrimsson B, Green RM, Katz DC, Fish JL, Bernier FP, Roseman CC, Young NM, Cheverud JM, Marcucio RS. The developmental-genetics of canalization. Semin Cell Dev Biol. 2019 Apr;88:67-79. doi: 10.1016/j.semcdb.2018.05.019. Epub 2018 May 24. PMID: 29782925; PMCID: PMC6251770.

[7] Takahashi KH. Multiple modes of canalization: Links between genetic, environmental canalizations and developmental stability, and their trait-specificity. Semin Cell Dev Biol. 2019 Apr;88:14-20. doi: 10.1016/j.semcdb.2018.05.018. Epub 2018 May 22. PMID: 29787862.

[8] Garelli A, Gontijo AM, Miguela V, Caparros E, Dominguez M. Imaginal discs secrete insulin-like peptide 8 to mediate plasticity of growth and maturation. Science. 2012 May 4;336(6081):579-82. doi: 10.1126/science.1216735.

[9] Colombani J, Andersen D, Leopold P. Secreted peptide Dilp8 coordinates Drosophila tissue growth with developmental timing. Science. 2012 May 4;336(6081):582-5. doi: 10.1126/science.1216689

[10] Gontijo AM, Garelli A. The biology and evolution of the Dilp8-Lgr3 pathway: A relaxin-like pathway coupling tissue growth and developmental timing control. Mech Dev. 2018 Dec:154:44-50. doi: 10.1016/j.mod.2018.04.005. Epub 2018 Apr 30.

[11] Simpson P, Berreur P, Berreur-Bonnenfant J. The initiation of pupariation in Drosophila: dependence on growth of the imaginal discs. J Embryol Exp Morphol. 1980 Jun;57:155-65. PMID: 7430927.

[12] Hackney JF, Zolali-Meybodi O, Cherbas P. Tissue damage disrupts developmental progression and ecdysteroid biosynthesis in Drosophila. PLoS One. 2012;7(11):e49105. doi: 10.1371/journal.pone.0049105. Epub 2012 Nov 13. PMID: 23166607; PMCID: PMC3496736.

[13] Klebes A, Sustar A, Kechris K, Li H, Schubiger G, Kornberg TB. Regulation of cellular plasticity in Drosophila imaginal disc cells by the Polycomb group, trithorax group and lama genes. Development. 2005 Aug;132(16):3753-65. doi: 10.1242/dev.01927. Erratum in: Development. 2005 Oct;132(19):4419. PMID: 16077094.

[14] Demay Y, Perochon J, Szuplewski S, Mignotte B, Gaumer S. The PERK pathway independently triggers apoptosis and a Rac1/Slpr/JNK/Dilp8 signaling favoring tissue homeostasis in a chronic ER

stress Drosophila model. Cell Death Dis. 2014 Oct 9;5(10):e1452. doi: 10.1038/cddis.2014.403. PMID: 25299777; PMCID: PMC4649510.

[15] Katsuyama T, Comoglio F, Seimiya M, Cabuy E, Paro R. During Drosophila disc regeneration, JAK/STAT coordinates cell proliferation with Dilp8-mediated developmental delay. Proc Natl Acad Sci U S A. 2015 May 5;112(18):E2327-36. doi: 10.1073/pnas.1423074112. Epub 2015 Apr 20. PMID: 25902518; PMCID: PMC4426433.

[16] Colombani J, Andersen D, Boulan L, Boone E, Romero N, Virolle V, Texada M, Leopold P. Drosophila Lgr3 Couples Organ Growth with Maturation and Ensures Developmental Stability. Curr Biol. 2015 Oct 19;25(20):2723-9. doi: 10.1016/j.cub.2015.09.020. Epub 2015 Oct 1.

[17] Garelli A, Heredia F, Casimiro AP, Macedo A, Nunes C, Garcez M, Dias ARM, Volonte YA, Uhlmann T, Caparros E, Koyama T, Gontijo AM. Dilp8 requires the neuronal relaxin receptor Lgr3 to couple growth to developmental timing. Nat Commun. 2015 Oct 29;6:8732. doi: 10.1038/ncomms9732. PMID: 26510564; PMCID: PMC4640092.

[18] Vallejo DM, Juarez-Carreño S, Bolivar J, Morante J, Dominguez M. A brain circuit that synchronizes growth and maturation revealed through Dilp8 binding to Lgr3. Science. 2015 Nov 13;350(6262):aac6767. doi: 10.1126/science.aac6767. Epub 2015 Oct 1. PMID: 26429885.

[19] Jaszczak JS, Wolpe JB, Bhandari R, Jaszczak RG, Halme A. Growth Coordination During Drosophila melanogaster Imaginal Disc Regeneration Is Mediated by Signaling Through the Relaxin Receptor Lgr3 in the Prothoracic Gland. Genetics. 2016 Oct;204(2):703-709. doi: 10.1534/genetics.116.193706. Epub 2016 Aug 24. PMID: 27558136; PMCID: PMC5068856.

[20] Jenett A, Rubin GM, Ngo TT, Shepherd D, Murphy C, Dionne H, Pfeiffer BD, Cavallaro A, Hall D, Jeter J, Iyer N, Fetter D, Hausenfluck JH, Peng H, Trautman ET, Svirskas RR, Myers EW, Iwinski ZR, Aso Y, DePasquale GM, Enos A, Hulamm P, Lam SC, Li HH, Laverty TR, Long F, Qu L, Murphy SD, Rokicki K, Safford T, Shaw K, Simpson JH, Sowell A, Tae S, Yu Y, Zugates CT. A GAL4-driver line resource for Drosophila neurobiology. Cell Rep. 2012 Oct 25;2(4):991-1001. doi: 10.1016/j.celrep.2012.09.011. Epub 2012 Oct 11. PMID: 23063364; PMCID: PMC3515021.

[21] Ito K, Sass H, Urban J, Hofbauer A, Schneuwly S. GAL4-responsive UAS-tau as a tool for studying the anatomy and development of the Drosophila central nervous system. Cell Tissue Res. 1997 Oct;290(1):1-10. doi: 10.1007/s004410050901. PMID: 9377629.

[22] Johns DC, Marx R, Mains RE, O'Rourke B, Marbán E. Inducible genetic suppression of neuronal excitability. J Neurosci. 1999 Mar 1;19(5):1691-7. doi: 10.1523/JNEUROSCI.19-05-01691.1999. PMID: 10024355; PMCID: PMC6782162.

[23] Baines RA, Uhler JP, Thompson A, Sweeney ST, Bate M. Altered electrical properties in Drosophila neurons developing without synaptic transmission. J Neurosci. 2001 Mar 1;21(5):1523-31. doi: 10.1523/JNEUROSCI.21-05-01523.2001. PMID: 11222642; PMCID: PMC6762927.

[24] Rogulja D, Young MW. Control of sleep by cyclin A and its regulator. Science. 2012 Mar 30;335(6076):1617-21. doi: 10.1126/science.1212476. PMID: 22461610.

[25] Afonso DJ, Liu D, Machado DR, Pan H, Jepson JE, Rogulja D, Koh K. TARANIS Functions with Cyclin A and Cdk1 in a Novel Arousal Center to Control Sleep in Drosophila. Curr Biol. 2015 Jun 29;25(13):1717-26. doi: 10.1016/j.cub.2015.05.037. Epub 2015 Jun 18. PMID: 26096977; PMCID: PMC4559600.

[26] Ramirez JM, Tryba AK, Peña F. Pacemaker neurons and neuronal networks: an integrative view. Curr Opin Neurobiol. 2004 Dec;14(6):665-74. doi: 10.1016/j.conb.2004.10.011. PMID: 15582367.

[27] Marder E, Goeritz ML, Otopalik AG. Robust circuit rhythms in small circuits arise from variable circuit components and mechanisms. Curr Opin Neurobiol. 2015 Apr;31:156-63. doi: 10.1016/j.conb.2014.10.012. Epub 2014 Nov 6. PMID: 25460072; PMCID: PMC4375070.

[28] Li HH, Kroll JR, Lennox SM, Ogundeyi O, Jeter J, Depasquale G, Truman JW. A GAL4 driver resource for developmental and behavioral studies on the larval CNS of Drosophila. Cell Rep. 2014 Aug 7;8(3):897-908. doi: 10.1016/j.celrep.2014.06.065. Epub 2014 Jul 31. PMID: 25088417.

[29] Meissner GW, Luo SD, Dias BG, Texada MJ, Baker BS. Sex-specific regulation of Lgr3 in Drosophila neurons. Proc Natl Acad Sci U S A. 2016 Mar 1;113(9):E1256-65. doi: 10.1073/pnas.1600241113. Epub 2016 Feb 16. PMID: 26884206; PMCID: PMC4780643.

[30] Ni JQ, Zhou R, Czech B, Liu LP, Holderbaum L, Yang-Zhou D, Shim HS, Tao R, Handler D, Karpowicz P, Binari R, Booker M, Brennecke J, Perkins LA, Hannon GJ, Perrimon N. A genome-scale shRNA resource for transgenic RNAi in Drosophila. Nat Methods. 2011 May;8(5):405-7. doi: 10.1038/nmeth.1592. Epub 2011 Apr 3. PMID: 21460824; PMCID: PMC3489273.

[31] Pfeiffer BD, Ngo TT, Hibbard KL, Murphy C, Jenett A, Truman JW, Rubin GM. Refinement of tools for targeted gene expression in Drosophila. Genetics. 2010 Oct;186(2):735-55. doi: 10.1534/genetics.110.119917. Epub 2010 Aug 9. PMID: 20697123; PMCID: PMC2942869.

[32] Hong JW, Hendrix DA, Levine MS. Shadow enhancers as a source of evolutionary novelty. Science. 2008 Sep 5;321(5894):1314. doi: 10.1126/science.1160631. PMID: 18772429; PMCID: PMC4257485.

[33] Cannavò E, Khoueiry P, Garfield DA, Geeleher P, Zichner T, Gustafson EH, Ciglar L, Korbel JO, Furlong EE. Shadow Enhancers Are Pervasive Features of Developmental Regulatory Networks. Curr Biol. 2016 Jan 11;26(1):38-51. doi: 10.1016/j.cub.2015.11.034. Epub 2015 Dec 10. PMID: 26687625; PMCID: PMC4712172.

[34] Viswanath V, Story GM, Peier AM, Petrus MJ, Lee VM, Hwang SW, Patapoutian A, Jegla T. Opposite thermosensor in fruitfly and mouse. Nature. 2003 Jun 19;423(6942):822-3. doi: 10.1038/423822a. PMID: 12815418.

[35] Hamada FN, Rosenzweig M, Kang K, Pulver SR, Ghezzi A, Jegla TJ, Garrity PA. An internal thermal sensor controlling temperature preference in Drosophila. Nature. 2008 Jul 10;454(7201):217-20. doi: 10.1038/nature07001. Epub 2008 Jun 11. PMID: 18548007; PMCID: PMC2730888.

[36] Parisky KM, Agosto J, Pulver SR, Shang Y, Kuklin E, Hodge JJ, Kang K, Liu X, Garrity PA, Rosbash M, Griffith LC. PDF cells are a GABA-responsive wake-promoting component of the Drosophila sleep circuit. Neuron. 2008 Nov 26;60(4):672-82. doi: 10.1016/j.neuron.2008.10.042. Erratum in: Neuron. 2009 Jan 15;61(1):152. Kang, Keongjin [corrected to Kang, Kyeongjin]. PMID: 19038223; PMCID: PMC2734413.

[37] Pulver SR, Pashkovski SL, Hornstein NJ, Garrity PA, Griffith LC. Temporal dynamics of neuronal activation by Channelrhodopsin-2 and TRPA1 determine behavioral output in Drosophila larvae. J Neurophysiol. 2009 Jun;101(6):3075-88. doi: 10.1152/jn.00071.2009. Epub 2009 Apr 1. PMID: 19339465; PMCID: PMC2694103.

[38] Maldonado-Díaz C, Vazquez M, Marie B. A comparison of three different methods of eliciting rapid activity-dependent synaptic plasticity at the Drosophila NMJ. PLoS One. 2021 Nov 30;16(11):e0260553. doi: 10.1371/journal.pone.0260553. PMID: 34847197; PMCID: PMC8631638.

[39] Nern A, Pfeiffer BD, Svoboda K, Rubin GM. Multiple new site-specific recombinases for use in manipulating animal genomes. Proc Natl Acad Sci U S A. 2011 Aug 23;108(34):14198-203. doi: 10.1073/pnas.1111704108. Epub 2011 Aug 9. PMID: 21831835; PMCID: PMC3161616.

[40] Bohm RA, Welch WP, Goodnight LK, Cox LW, Henry LG, Gunter TC, Bao H, Zhang B. A genetic mosaic approach for neural circuit mapping in Drosophila. Proc Natl Acad Sci U S A. 2010 Sep 14;107(37):16378-83. doi: 10.1073/pnas.1004669107. Epub 2010 Sep 1. PMID: 20810922; PMCID: PMC2941334.

[41] Clyne JD, Miesenböck G. Sex-specific control and tuning of the pattern generator for courtship song in Drosophila. Cell. 2008 Apr 18;133(2):354-63. doi: 10.1016/j.cell.2008.01.050. PMID: 18423205.

[42] Birnbaumer L. Chapter 197 - Signal Transduction by G Proteins: Basic Principles, Molecular Diversity, and Structural Basis of Their Actions. In: Handbook of Cell Signaling (Second Edition), Academic Press, Editor(s): Ralph A. Bradshaw, Edward A. Dennis, 2010, 1597-614.

[43] Luo L. Principles of Neurobiology (2nd ed.). Garland Science. 2020. https://doi.org/10.1201/9781003053972

[44] Yang CH, Rumpf S, Xiang Y, Gordon MD, Song W, Jan LY, Jan YN. Control of the postmating behavioral switch in Drosophila females by internal sensory neurons. Neuron. 2009 Feb 26;61(4):519-26. doi: 10.1016/j.neuron.2008.12.021. PMID: 19249273; PMCID: PMC2748846.

[45] Koenig JH, Saito K, Ikeda K. Reversible control of synaptic transmission in a single gene mutant of Drosophila melanogaster. J Cell Biol. 1983 Jun;96(6):1517-22. doi: 10.1083/jcb.96.6.1517. PMID: 6304107; PMCID: PMC2112451.

[46] Sweeney ST, Broadie K, Keane J, Niemann H, O'Kane CJ. Targeted expression of tetanus toxin light chain in Drosophila specifically eliminates synaptic transmission and causes behavioral defects. Neuron. 1995 Feb;14(2):341-51. doi: 10.1016/0896-6273(95)90290-2. PMID: 7857643.

[47] Stockinger P, Kvitsiani D, Rotkopf S, Tirián L, Dickson BJ. Neural circuitry that governs Drosophila male courtship behavior. Cell. 2005 Jun 3;121(5):795-807. doi: 10.1016/j.cell.2005.04.026. PMID: 15935765.

[48] von Philipsborn AC, Liu T, You JY, Masser C, Bidaye SS, Dickson BJ. Neuronal Control of Drosophila Courtship Song. Neuron. 2011 Feb 10;69(3):509-22. doi: 10.1016/j.neuron.2011.01.011.

[49] Gerhard S, Andrade I, Fetter RD, Cardona A, Schneider-Mizell CM. Conserved neural circuit structure across Drosophila larval development revealed by comparative connectomics. Elife. 2017 Oct 23;6:e29089. doi: 10.7554/eLife.29089. PMID: 29058674; PMCID: PMC5662290.

[50] Derjean D, Bertrand S, Le Masson G, Landry M, Morisset V, Nagy F. Dynamic balance of metabotropic inputs causes dorsal horn neurons to switch functional states. Nat Neurosci. 2003 Mar;6(3):274-81. doi: 10.1038/nn1016. PMID: 12592405.

[51] Baccei ML. Pacemaker Neurons and the Development of Nociception. Neuroscientist. 2014 Jun;20(3):197-202. doi: 10.1177/1073858414521499. Epub 2014 Feb 7. PMID: 24510073; PMCID: PMC4927414.

[52] Ifshin MS, Gainer H, Barker JL. Peptide factor extracted from molluscan ganglia that modulates bursting pacemaker activity. Nature. 1975 Mar 6;254(5495):72-4. doi: 10.1038/254072a0. PMID: 1113880.

[53] Van Soest PF, Lodder JC, Kits KS. Activation of protein kinase C by oxytocin-related conopressin underlies pacemaker current in Lymnaea central neurons. J Neurophysiol. 2000 Nov;84(5):2541-51. doi: 10.1152/jn.2000.84.5.2541. PMID: 11067996.

[54] Reppert SM, Weaver DR. Coordination of circadian timing in mammals. Nature. 2002 Aug 29;418(6901):935-41. doi: 10.1038/nature00965. PMID: 12198538.

[55] Kaneko M, Helfrich-Förster C, Hall JC. Spatial and temporal expression of the period and timeless genes in the developing nervous system of Drosophila: newly identified pacemaker candidates and novel features of clock gene product cycling. J Neurosci. 1997 Sep 1;17(17):6745-60. doi: 10.1523/JNEUROSCI.17-17-06745.1997. PMID: 9254686; PMCID: PMC6573141.

[56] Hardin PE. Molecular genetic analysis of circadian timekeeping in Drosophila. Adv Genet. 2011;74:141-73. doi: 10.1016/B978-0-12-387690-4.00005-2. PMID: 21924977; PMCID: PMC4108082.

[57] Kaneko M, Hall JC. Neuroanatomy of cells expressing clock genes in Drosophila: transgenic manipulation of the period and timeless genes to mark the perikarya of circadian pacemaker neurons and their projections. J Comp Neurol. 2000 Jun 19;422(1):66-94. doi: 10.1002/(sici)1096-9861(20000619)422:1<66::aid-cne5>3.0.co;2-2. PMID: 10842219.

[58] Helfrich-Förster C. The period clock gene is expressed in central nervous system neurons which also produce a neuropeptide that reveals the projections of circadian pacemaker cells within the brain of Drosophila melanogaster. Proc Natl Acad Sci U S A. 1995 Jan 17;92(2):612-6. doi: 10.1073/pnas.92.2.612. PMID: 7831339; PMCID: PMC42792.

[59] Mertens I, Vandingenen A, Johnson EC, Shafer OT, Li W, Trigg JS, De Loof A, Schoofs L, Taghert PH. PDF receptor signaling in Drosophila contributes to both circadian and geotactic behaviors. Neuron. 2005 Oct 20;48(2):213-9. doi: 10.1016/j.neuron.2005.09.009. PMID: 16242402.

[60] Im SH, Taghert PH. PDF receptor expression reveals direct interactions between circadian oscillators in Drosophila. J Comp Neurol. 2010 Jun 1;518(11):1925-45. doi: 10.1002/cne.22311. PMID: 20394051; PMCID: PMC2881544.

[61] Lehner CF, O'Farrell PH. Expression and function of Drosophila cyclin A during embryonic cell cycle progression. Cell. 1989 Mar 24;56(6):957-68. doi: 10.1016/0092-8674(89)90629-6. PMID: 2564316; PMCID: PMC2753420.

[62] Murray A, Hunt T. The Cell Cycle: An Introduction. W. H. Freeman and Company, New York. 1993.

[63] Heredia F, Volonté Y, Pereirinha J, Fernandez-Acosta M, Casimiro AP, Belém CG, Viegas F, Tanaka K, Menezes J, Arana M, Cardoso GA, Macedo A, Kotowicz M, Prado Spalm FH, Dibo MJ, Monfardini RD, Torres TT, Mendes CS, Garelli A, Gontijo AM. The steroid-hormone ecdysone coordinates parallel pupariation neuromotor and morphogenetic subprograms via epidermis-to-neuron Dilp8-Lgr3 signal induction. Nat Commun. 2021 Jun 7;12(1):3328. doi: 10.1038/s41467-021-23218-5. PMID: 34099654; PMCID: PMC8184853.

[64] Nandakumar S, Grushko O, Buttitta LA. Polyploidy in the adult *Drosophila* brain. Elife. 2020 Aug 25;9:e54385. doi: 10.7554/eLife.54385. PMID: 32840209; PMCID: PMC7447450.

[65] Nern A, Rubin GM. Optimized tools for multicolor stochastic labeling reveal diverse stereotyped cell arrangements in the fly visual system. Proc. Natl. Acad. Sci. U.S.A. 2015 112(22): E2967--E2976.

[66] Winding M, Pedigo BD, Barnes CL, Patsolic HG, Park Y, Kazimiers T, Fushiki A, Andrade IV, Khandelwal A, Valdes-Aleman J, Li F, Randel N, Barsotti E, Correia A, Fetter RD, Hartenstein V, Priebe CE, Vogelstein JT, Cardona A, Zlatic M. The connectome of an insect brain. Science. 2023 Mar 10;379(6636):eadd9330. doi: 10.1126/science.add9330. Epub 2023 Mar 10. PMID: 36893230; PMCID: PMC7614541.

[67] Wagh DA, Rasse TM, Asan E, Hofbauer A, Schwenkert I, Dürrbeck H, Buchner S, Dabauvalle MC, Schmidt M, Qin G, Wichmann C, Kittel R, Sigrist SJ, Buchner E. Bruchpilot, a protein with homology to ELKS/CAST, is required for structural integrity and function of synaptic active zones in Drosophila. Neuron. 2006 Mar 16;49(6):833-44. doi: 10.1016/j.neuron.2006.02.008. Erratum in: Neuron. 2006 Jul 20;51(2):275. PMID: 16543132.

[68] Chen Y, Akin O, Nern A, Tsui CY, Pecot MY, Zipursky SL. Cell-type-specific labeling of synapses in vivo through synaptic tagging with recombination. Neuron. 2014 Jan 22;81(2):280-93. doi: 10.1016/j.neuron.2013.12.021. PMID: 24462095; PMCID: PMC4025979.

[69] Zhang YQ, Rodesch CK, Broadie K. Living synaptic vesicle marker: synaptotagmin-GFP. Genesis. 2002 Sep-Oct;34(1-2):142-5. doi: 10.1002/gene.10144. PMID: 12324970.

[70] Nicolaï LJ, Ramaekers A, Raemaekers T, Drozdzecki A, Mauss AS, Yan J, Landgraf M, Annaert W, Hassan BA. Genetically encoded dendritic marker sheds light on neuronal connectivity in Drosophila. Proc Natl Acad Sci U S A. 2010 Nov 23;107(47):20553-8. doi: 10.1073/pnas.1010198107. Epub 2010 Nov 8. PMID: 21059961; PMCID: PMC2996714.

[71] McCormick DA, Nestvogel DB, He BJ. Neuromodulation of Brain State and Behavior. Annu Rev Neurosci. 2020 Jul 8;43:391-415. doi: 10.1146/annurev-neuro-100219-105424. Epub 2020 Apr 6. PMID: 32250724.

[72] Feldman J. The neural binding problem(s). Cogn Neurodyn. 2013 Feb;7(1):1-11. doi: 10.1007/s11571-012-9219-8. Epub 2012 Sep 1. PMID: 24427186; PMCID: PMC3538094.

[73] Fries P, Reynolds JH, Rorie AE, Desimone R. Modulation of oscillatory neuronal synchronization by selective visual attention. Science. 2001; 291(5508):1560–1563.

[74] Engel AK, Fries P, Singer W. Dynamic predictions: oscillations and synchrony in top-down processing. Nat Rev Neurosci. 2001 Oct;2(10):704-16. doi: 10.1038/35094565. PMID: 11584308.

[75] Lewis CM, Wunderle T, Fries P. Top-down modulation of visual cortical stimulus encoding and gamma independent of firing rates. bioRxiv [Preprint]. 2024 Apr 12:2024.04.11.589006. doi: 10.1101/2024.04.11.589006. PMID: 38645050; PMCID: PMC11030389.

[76] de Velasco B, Erclik T, Shy D, Sclafani J, Lipshitz H, McInnes R, Hartenstein V. Specification and development of the pars intercerebralis and pars lateralis, neuroendocrine command centers in the Drosophila brain. Dev Biol. 2007 Feb 1;302(1):309-23. doi: 10.1016/j.ydbio.2006.09.035. Epub 2006 Sep 26. PMID: 17070515.

[77] Swanson LW. Cerebral hemisphere regulation of motivated behavior. Brain Res. 2000 Dec 15;886(1-2):113-164. doi: 10.1016/s0006-8993(00)02905-x. PMID: 11119693.

[78] Jennings JH, Ung RL, Resendez SL, Stamatakis AM, Taylor JG, Huang J, Veleta K, Kantak PA, Aita M, Shilling-Scrivo K, Ramakrishnan C, Deisseroth K, Otte S, Stuber GD. Visualizing hypothalamic network dynamics for appetitive and consummatory behaviors. Cell. 2015 Jan 29;160(3):516-27. doi: 10.1016/j.cell.2014.12.026. PMID: 25635459; PMCID: PMC4312416.

[79] Kennedy A, Kunwar PS, Li LY, Stagkourakis S, Wagenaar DA, Anderson DJ. Stimulus-specific hypothalamic encoding of a persistent defensive state. Nature. 2020 Oct;586(7831):730-734. doi: 10.1038/s41586-020-2728-4. Epub 2020 Sep 16. PMID: 32939094; PMCID: PMC7606611.

[80] Chen C, Altafi M, Corbu MA, Trenk A, van den Munkhof H, Weineck K, Bender F, Carus-Cadavieco M, Bakhareva A, Korotkova T, Ponomarenko A. The dynamic state of a prefrontal-hypothalamic-midbrain circuit commands behavioral transitions. Nat Neurosci. 2024 May;27(5):952-963. doi: 10.1038/s41593-024-01598-3. Epub 2024 Mar 18. PMID: 38499854; PMCID: PMC11089001.

[81] Schweitzer P, Madamba SG, Siggins GR. The sleep-modulating peptide cortistatin augments the h-current in hippocampal neurons. J Neurosci. 2003 Nov 26;23(34):10884-91. doi: 10.1523/JNEUROSCI.23-34-10884.2003. PMID: 14645483; PMCID: PMC6740974.

[82] Marder E, Bucher D. Central pattern generators and the control of rhythmic movements. Curr Biol. 2001 Nov 27;11(23):R986-96. doi: 10.1016/s0960-9822(01)00581-4. PMID: 11728329.

[83] Ma S, Olucha-Bordonau FE, Hossain MA, Lin F, Kuei C, Liu C, Wade JD, Sutton SW, Nuñez A, Gundlach AL. Modulation of hippocampal theta oscillations and spatial memory by relaxin-3 neurons of the nucleus incertus. Learn Mem. 2009 Oct 30;16(11):730-42. doi: 10.1101/lm.1438109. PMID: 19880588.

[84] Albert-Gascó H, Ma S, Ros-Bernal F, Sánchez-Pérez AM, Gundlach AL, Olucha-Bordonau FE. GABAergic Neurons in the Rat Medial Septal Complex Express Relaxin-3 Receptor (RXFP3) mRNA. Front Neuroanat. 2018 Jan 17;11:133. doi: 10.3389/fnana.2017.00133. PMID: 29403361; PMCID: PMC5777284.

[85] Koyama T, Texada MJ, Halberg KA, Rewitz K. Metabolism and growth adaptation to environmental conditions in Drosophila. Cell Mol Life Sci. 2020 Nov;77(22):4523-4551. doi: 10.1007/s00018-020-03547-2. Epub 2020 May 24. PMID: 32448994; PMCID: PMC7599194.

[86] Imura E, Shimada-Niwa Y, Nishimura T, Hückesfeld S, Schlegel P, Ohhara Y, Kondo S, Tanimoto H, Cardona A, Pankratz M, Niwa R. The Corazonin-PTTH Neuronal Axis Controls Systemic Body Growth by Regulating Basal Ecdysteroid Biosynthesis in Drosophila melanogaster. Curr Biol.2020 June 8, 30, 2156–2165. DOI: 10.1016/j.cub.2020.03.050

[87] Pan X, O'Connor MB. Coordination among multiple receptor tyrosine kinase signals controls Drosophila developmental timing and body size. Cell Rep. 2021 Aug 31;36(9):109644. doi: 10.1016/j.celrep.2021.109644. PMID: 34469735; PMCID: PMC8428980.

[88] McBrayer Z, Ono H, Shimell M, Parvy JP, Beckstead RB, Warren JT, Thummel CS, Dauphin-Villemant C, Gilbert LI, O'Connor MB. Prothoracicotropic hormone regulates developmental timing and body size in Drosophila. Dev Cell. 2007 Dec;13(6):857-71. doi: 10.1016/j.devcel.2007.11.003. PMID: 18061567; PMCID: PMC2359579.

[89] Rewitz KF, Yamanaka N, Gilbert LI, O'Connor MB. The insect neuropeptide PTTH activates receptor tyrosine kinase torso to initiate metamorphosis. Science. 2009 Dec 4;326(5958):1403-5. doi: 10.1126/science.1176450. PMID: 19965758.

[90] Halme A, Cheng M, Hariharan IK. Retinoids regulate a developmental checkpoint for tissue regeneration in Drosophila. Curr Biol. 2010 Mar 9;20(5):458-63. doi: 10.1016/j.cub.2010.01.038. PMID: 20189388; PMCID: PMC2847081.

[91] Casso D, Ramirez-Weber F, Kornberg TB. GFP-tagged balancer chromosomes for Drosophila melanogaster. Mech. Dev. 1999 88(2): 229-232. doi: 10.1016/s0925-4773(99)00174-4 PMID: 1053462

[92] Schindelin J, Arganda-Carreras I, Frise E, Kaynig V, Longair M, Pietzsch T, Preibisch S, Rueden C, Saalfeld S, Schmid B, Tinevez JY, White DJ, Hartenstein V, Eliceiri K, Tomancak P, Cardona A. Fiji: an open-source platform for biological-image analysis. Nat Methods. 2012 Jun 28;9(7):676-82. doi: 10.1038/nmeth.2019. PMID: 22743772; PMCID: PMC3855844.